Taphonomy and palaeoecology of the lower Miocene marine vertebrate assemblage of Ullujaya (Chilcatay Formation, East Pisco Basin, southern Peru)

Giovanni Bianucci[1,*], Alberto Collareta[1], Giulia Bosio[2], Walter Landini[1], Karen Gariboldi[1], Anna Gioncada[1], Olivier Lambert[3], Elisa Malinverno[2], Christian de Muizon[4], Rafael Varas-Malca[5], Igor Maria Villa[2], Giovanni Coletti[2], Mario Urbina[5], Claudio Di Celma[6]

[1] Dipartimento di Scienze della Terra, Università di Pisa, 56126 Pisa, Italy

[2] Dipartimento di Scienze dell'Ambiente e della Terra, Università di Milano Bicocca, 20126 Milano, Italy

[3] D.O. Terre et Histoire de la Vie, Institut Royal des Sciences Naturelles de Belgique, 1000 Brussels, Belgium

[4] Département Origines et Évolution, Muséum National d'Histoire Naturelle, Centre de Recherches sur la paléobiodiversité et les paléoenvironnements – CR2P (CNRS, MNHN, Sorbonne Université), 75005 Paris, France

[5] Departamento de Paleontologia de Vertebrados, Museo de Historia Natural de la Universidad Nacional Mayor de San Marcos, avenida Arenales 1256, Lima 14, Peru

[6] Scuola di Scienze e Tecnologie, Università di Camerino, 62032 Camerino, Italy

** Corresponding author. E-mail address: bianucci@dst.unipi.it*

Abstract

The taphonomy and palaeoecology of the early Miocene (Burdigalian) vertebrate assemblage of Ullujaya (East Pisco Basin, Peru) is here described. Vertebrate remains are concentrated in marine facies (*Ct1a* association) of the exposed Chilcatay Formation (dated 19-18 Ma) deposited within a 30-40 m deep, semi-enclosed, offshore environment. Coupled with ichnological observations, the size distribution of pyrite framboid relics reveals fluctuation of euxinic and oxic-dysoxic conditions at the seafloor. The assemblage is dominated by toothed cetaceans (kentriodontids, squalodelphinids, physeteroids, and the eurhinodelphinid-like *Chilcacetus*), together with a large dermochelyid turtle, some bony fish, and diverse elasmobranchs, mostly juveniles of *Carcharhinus brachyurus* and *Cosmopolitodus hastalis*. The vertebrate assemblage comprises a coastal community, dominated by mesopredators, representative of a warm-temperate, sheltered embayment connected with riverine and open-ocean environments. Vertebrate skeletons are typically disarticulated and incomplete, and some bone elements display shark bite marks. Microborings are observed at the bone surface. Bones exhibit a good degree of apatite mineralisation and bone cavities are locally filled by Ca-Mg carbonates. Our taphonomic observations suggest prolonged flotation of carcasses during which they were subject to biogenic and physical processes of partial destruction (including scavenging by sharks), before final deposition on a soft compact substrate. Preservation was favoured by the oxygen-deficient bottom conditions that inhibited the action of benthic macro-scavengers.

Keywords

Burdigalian, Cetacea, Elasmobranchii, Fossil-Lagerstätte, palaeoenvironments, taphonomy.

1. Introduction

Remarkable global climatic, oceanographic, and seal-level changes occurred during the

Cenozoic, promoting the redistribution and partitioning of food resources and consequent changes in diversity and disparity of marine vertebrates (Norris et al., 2013). Although some general models linking these environmental changes to the evolution of different marine vertebrate lineages have already been proposed (Marx and Uhen 2010), our knowledge of Cenozoic marine vertebrates is still primarily based on a chronostratigraphically and geographically heterogeneous fossil record. For these reasons, the reliability of such models in depicting global evolutionary trends has been questioned (Pyenson et al., 2010).

Contrasting with this fragmentary global scenario, the Eocene to Pliocene fill of the East Pisco Basin, southern coast of Peru (hereinafter: EPB), features one of the largest concentrations of Cenozoic marine vertebrate fossils discovered worldwide. The fossil content of the (?)middle Miocene to Pliocene Pisco Formation, the youngest portion of the basin fill, is well-known from a systematic, palaeoecological and taphonomic point of view, based on thirty-five years of research efforts (see Bianucci et al. 2016a, b and Di Celma et al. 2017 for a complete reference list). Besides strongly contributing to the clarification of several aspects of the Neogene global evolutionary trends for several marine vertebrate lineages, these studies also provided insights into the genesis of the extraordinary fossil assemblage of the Pisco Formation. By contrast, the knowledge on the fossil contents of the older deposits of the EPB is still fragmentary, although including some specimens of extraordinary relevance, for both their evolutionary significance and their exceptional preservation (e.g., Clarke et al, 2010; Uhen et al., 2011; Lambert et al. 2017a; Martínez-Cáceres et al., 2017). Moreover, studies carried out in the last years by our team highlighted an unexpected abundance of fossil vertebrates in the lower Miocene strata of the Chilcatay Formation.

All fossil vertebrates represented by bone elements described so far from this formation belong to odontocetes (toothed whales) and particularly to the platanistoid family Squalodelphinidae (Lambert et al. 2014; Bianucci et al., 2015, 2018), the new family Inticetidae (Lambert et al., 2018), and the longirostrine eurhinodelphid-like genus *Chilcacetus* (Lambert et al., 2015b). In addition, the

fossil assemblages of some shark tooth-rich beds have been described in detail (Landini et al., 2018).

Most of these fossils have been discovered in a few localities along the western side of the Ica River (e.g., Roca Negra, Ullujaya, and Zamaca), where the Chilcatay beds are extensively exposed. The aim of the present interdisciplinary work is to describe the marine vertebrate assemblage of one of these localities – Ullujaya – from a taphonomic and palaeoecological point of view in order to define the conditions and processes leading to the preservation of such a remarkable fossil record and to assess the ecological significance of this assemblage in the global evolutionary scenario of the Miocene marine vertebrate biota.

2. Tectono-stratigraphic context

Since Mesozoic times, the tectono-dynamics of Peru have been controlled by the convergence of the oceanic Nazca/Farallon Plate and the continental South American Plate. This transform-convergent margin, characterised by normal to strike-slip faults, formed elongated basins along the Peruvian forearc (Kulm et al., 1982; Dunbar et al., 1990; León et al., 2008; Zúñiga-Rivero et al., 2010; Viveen and Schlunegger, 2018) (Fig. 1). According to Thornburg and Kulm (1981), two long and narrow, trench-parallel structural highs - the Outer Shelf High and the Upper Slope Ridge - formed on the continental shelf and upper slope in Late Cretaceous–early Palaeogene times, segmenting the Peruvian offshore into an inner set of shelf basins and a seaward set of slope basins (Fig. 1A). In this frame, the onshore EPB lies east of the Outer Shelf High as a shelf basin, whereas the still-submerged West Pisco Basin lies west of the Outer Shelf High as an upper-slope basin. Active subduction erosion (von Huene and Lallemand, 1990; Clift et al., 2003; Hampel et al., 2004) controlled a prolonged period of normal faulting and subsidence in the EPB since at least the middle-late Eocene (Dunbar et al., 1990; León et al., 2008; Rustichelli et al., 2016a, b). This protracted extensional regime was only interrupted during the middle Miocene by a widespread

pulse of uplift, possibly related to the Quechua 1 tectonic event (Viveen and Schlunegger, 2018).

The sedimentary fill of the EPB comprises, from the oldest to the youngest, the Eocene Caballas Formation and Paracas Group (including the Los Choros and Yumaque formations), the upper Oligocene–middle Miocene Chilcatay Formation, and the (?)middle Miocene–Pliocene Pisco Formation (Dunbar et al., 1990; DeVries, 1998, 2017; DeVries et al., 2017; DeVries and Jud, 2018). Some of these units are bounded by regionally extensive angular unconformities, which account for periods of subaerial exposure (DeVries, 1998). During deposition of the Chilcatay Formation, the EPB was a shallow-water, semi-enclosed embayment bounded to the east by the Coastal Batholith (a complex of igneous rocks mostly emplaced during the Late Cretaceous–early Eocene) and protected to the west by a chain of crystalline basement islands (Marocco and Muizon, 1988; the Gran Tablazo Archipelago of DeVries and Jud, 2018) (Fig. 1B).

3. Study area and methods

Ullujaya is a richly fossiliferous site located in the Ocucaje area, along the western side of the Ica River, in the southern coastal desert of Peru (Fig. 1C). In this area, the Chilcatay Formation comprises two smaller units (namely, the Ct1 and Ct2 allomembers), separated by a major intraformational unconformity, CE0.2 (Figs. 2 and 3A). The stratigraphic interval of interest for the present study comprises the middle to upper part of the Ct1 allomember, since the older Ct1 strata and the unconformity at the base of the formation (CE0.1) are not exposed at Ullujaya. By using a 66-m-long measured section and a high-resolution geological map (Fig. 2), the vertebrate fossil assemblages of the Chilcatay Formation exposed in this area have already been placed into a proper sedimentological, stratigraphic, and chronostratigraphic context by Di Celma et al. (2018).

Twenty-three sediment samples were collected along the measured section for palaeoecological, sedimentological, and chronostratigraphic purposes. Smear slides of fine-grained sediments were analysed with an Olympus BX50 polarised optical microscope. Diatoms and silicoflagellates were

analysed at 1000x. Some samples were analysed using a ZEISS Scanning Electron Microscope, after carbon coating. The size distribution of relics of pyrite framboids was used as an indicator of redox conditions (Wilkin et al., 1996). For the chronostratigraphic study, biotite phenocrysts from a tephra deposit were analysed for major elements using a JEOL 8200 Super Probe at the University of Milan to check for alteration. $^{40}Ar/^{39}Ar$ analyses were performed on hand-picked biotite crystals at the University of Milano-Bicocca, with the NuInstruments™ Noblesse® noble gas mass spectrometer, using an updated procedure based on Villa et al. (2000). The sample was irradiated avoiding Cd shielding in the nuclear reactor at the McMaster University (Canada); the Fish Canyon sanidine was used as flux monitor (assumed age: 28.172 ± 0.028 Ma, Rivera et al., 2011).

Macroscopic taphonomic data were collected both in the field and at the Museo de Historia Natural de la Universidad Nacional Mayor de San Marcos (hereinafter: MUSM) by examining fossils collected over the past years from the Ullujaya locality. Field observations were limited by the fact that most of the exposed specimens are still included in partially lithified sediment that has not been removed to avoid damaging the bones. Moreover, recent erosion partially destroyed and/or displaced the exposed bones. For selecting, describing, and quantifying this taphonomic information we also considered previous studies about the taphonomy of fossil vertebrates, with particular attention to the few papers dealing with marine mammal assemblages (e.g., Boessenecker et al., 2014, Danise and Dominici, 2014; Esperante et al. 2015). The articulation degree of associated bones was coded with numbers from 4 to 1 as follows: 4 (100-75% bones articulated); 3 (75-50%); 2 (50-25%); 1 (>25%); 0 (fully disarticulated bones). Similarly, for skeletal completeness: 4 (100-75% of the skeleton preserved); 3 (75-50%); 2 (50-25%); 1 (< 25%); 0 (one bone or one skeletal element, e.g. the cranium, preserved). Articulation and completeness of the cetacean skeletons were also quantitatively evaluated by using an approach similar to that used by Beardmore et al. (2012) and Beardmore and Furrer (2016a,b) for marine reptiles. Degrees of articulation and completeness, expressed as percentages, were plotted on a bivariate bubble plot in Microsoft Excel. A best-fit

linear trend line, forced through the point corresponding to 100% completeness and 100% articulation (i.e., the 'taphonomic origin' of the data, reflecting the common condition of specimens at death), was obtained. The 'T-value' was then defined by the intersect of the aforementioned trend line with the completeness axis. Pearson's r^2 value, indicating the goodness of fit of the regression line, was also obtained with Excel. Finally, the Spearman rank-order correlation coefficient (rs) was calculated in PAST (PAlaeontological STatistics program; Hammer and Harper, 2001) for having a non-parametric measure of the strength of correlation between articulation and completeness. Given the significant differences between reptile and cetacean skeletons (e.g., the cranial bones of cetaceans are less subject to disarticulation than those of reptiles), and considering also the relatively small size of our dataset (we analysed 52 specimens, excluding the remains exhibiting significant recent erosion and/or skeletons not found *in situ*), differing from Beardmore et al. (2012) and Beardmore and Furrer (2016a,b), we did not divide the skeleton in distinct units for the purposes of the quantitative taphonomic analysis.

In the field, taphonomic observations concerned the degree of preservation of the cortical bone and vertebral processes, as well as the presence/absence of: 1) bone abrasion; 2) bone fractures; 3) associated mollusc shells, remains of crabs and other invertebrates, teleostean and elasmobranch teeth; 4) associated remains of encrusting epibionts; and 5) traces of invertebrates and vertebrates.

Shark bite marks were analysed using the morphological-genetic approach proposed by Cigala Fulgosi (1990) and modified by Bianucci et al. (2010b) and Collareta et al. (2017a), distinguishing five types of bite marks (Type I to V) on the basis of the producing impact.

For microscopic taphonomic features, nine bone samples from seven cetacean specimens were prepared as polished thin sections cut orthogonally to the elongation of the bone. They were analysed with Olympus BX50 and Leica Leitz Laborlux S transmitted light and Leica DM EP reflected light microscopes and with scanning electron microscopy and microanalysis (SEM-EDS; Tescan VEGA TS 5136 XM, University of Milano-Bicocca and the Philips -EDAX Genesis

University of Pisa), obtaining semi-quantitative composition results.

4. Results

4.1. Stratigraphy, sedimentology, and age of the Chilcatay Formation at Ullujaya

The exposed portion of the Ct1 allomember is about 56 m thick and comprises a distinct two-fold subdivision of sedimentary facies, which includes a sub-horizontal package of interbedded medium- to fine-grained sandstones, sandy siltstones and siltstones (*Ct1a* facies association) and a stack of clinoformed units having a mixed siliciclastic-carbonate composition (*Ct1b* facies association).

The bulk of *Ct1a* is characterised by the dominance of massive, medium- to fine-grained siliciclastic sandstones and siltstones (Fig. 3B) with rare occurrences of silicoflagellates and diatoms, dominated by genera that are typical of coastal settings (*Actinoptychus*, *Cocconeis*, *Delphineis*, *Grammatophora*, *Paralia*). The diluted coarse biogenic fraction is composed of small amounts of redeposited skeletal elements including barnacles and mollusc shells (mainly ostreids and pectinids), both occurring as fragments and complete specimens, and rare echinoids and calcareous worm tubes. Rare encrusting bryozoans were observed on barnacle shells.

These fine-grained sediments are punctuated by laterally persistent beds of granule- to coarse-grained sandstones that range from 0.1 to 0.5 m in thickness and, locally, pass laterally into erosionally based cobble- to boulder-sized conglomerates up to 1.5 m thick. The bases of the granule- to coarse-grained sandstone beds are sharp and display dense burrow assemblages dominated by large *Thalassinoides* and subordinate *Gyrolithes* penetrating deeply into the subjacent fine-grained sediments (Figs. 3C, D). The burrows are backfilled with sediment from the overlying coarse-grained bed. The composition of the granule layers is a laterally variable mixture of siliciclastic grains, broken or whole shells of barnacles and small molluscs fragments, whereas that of the cobble- to boulder-sized conglomerates is dominated by rounded clasts from volcanic ash

196 tuffs and from the igneous basement set in a coarse-grained bioclastic matrix.

197 During microscopic observations, abundant, subspherical framboidal aggregates of Fe-
198 oxyhydroxide microcrystals, representing relic textures of pyrite framboids were detected through
199 the sediment, which consists of small rhombohedral crystals of dolomite terrigenous clasts, and
200 biogenic fragments (Fig. 4). The diameter of the framboids was measured in five samples from
201 *Ct1a*, selected between 22 and 28.5 m above the base of the measured section (abbreviated: abs),
202 where a high concentration of fossil vertebrates was found (Fig. 5). Framboids from 22 m abs, 23.5
203 m abs, 26 m abs, and 28.5 m abs exhibit a mean diameter of 4.6 ± 2.0 μm (as 1σ), 5.1 ± 1.9 μm, 5.3
204 ± 2.2 μm, and 5.0 ± 1.9 μm, respectively. Sample UL-D3 (25 m abs) exhibits a higher mean
205 diameter of 8.3 ± 4.8 μm. Framboids having a diameter greater than 10 μm are 3.8% at most except
206 for sample UL-D3 having a high percentage of large framboids (32.5%). Irregularly-shaped
207 framboids are rare and concentrated in sample UL-D3.

208 Sediments of *Ct1a* underlie and, locally, landward interfinger with a 20-m-thick, clinostratified
209 carbonate wedge (*Ct1b*). The dip direction of clinobeds is dominantly oriented to the southwest,
210 indicating a uniform progradation direction. Clinoform height attains 15-20 m and maximum
211 declivity ranges between 15° and 20°. Individual clinobeds are between 0.2 and 0.5 m thick and are
212 composed of coarse-grained, well-sorted, skeletal-rich grainstones mixed with subordinate amounts
213 of granule- and small pebble-sized terrigenous components. In terms of skeletal composition, *Ct1b*
214 is largely dominated by large-sized, hard-substrate-related shore barnacles, occurring either as
215 fragmented individuals or as clusters, with lesser amounts of molluscs, benthic foraminifera, and
216 echinoids, representing a typical heterozoan assemblage (*sensu* James, 1997). All shells exhibit a
217 high degree of fragmentation and disarticulation, and variably abraded shapes, indicative of
218 transport. The lower boundary of the clinobedded deposit is a downlap surface characterised by a
219 sharp and undulated lithologic contact with underlying sediments of *Ct1a*.

220 Diatom and silicoflagellate biostratigraphy already provides a robust chronology for the strata

exposed at Ullujaya and allows to define an age comprised between 18 and 19 Ma, with the age of the youngest portion of the section being in agreement with the $^{40}Ar/^{39}Ar$ age of 18.02 ± 0.07 Ma obtained from biotite in tephra SOT-T3, sampled just 1 m below the erosional contact with the overlying Pisco Formation (Di Celma et al., 2018). This chronostratigraphic framework is here further supported by a new $^{40}Ar/^{39}Ar$ dating of a volcanic ash layer (UJA-T35) sampled 2 m above the lowermost exposure of the Ct1 allomember at Ullujaya.

Although microprobe analyses on biotite phenocrysts from this ash layer highlighted a loss of K in the interlayer occupancy, it was one of the best preserved among the very few tephra detectable in the section. The isochemical steps probably circumvent the alteration and give a $^{40}Ar/^{39}Ar$ age of 19.00 ± 0.28 Ma (2σ uncertainty).

4.2. Overall composition of the fossil vertebrate assemblage

The assemblage includes bony vertebrates and chondrichthyan teeth. Eighty-two marine vertebrate specimens are preserved as bony elements (Table 1). Remains of Cetacea dominate this assemblage, accounting for 86.6% of the specimens, with a large number of indeterminate specimens (56.1%). All specimens identifiable to suborder level belong to Odontoceti and no baleen whale (Mysticeti) is recorded so far. Odontocete remains belong to Kentriodontidae (19.6%; early relatives of today's true dolphins and porpoises), Squalodelphinidae (6.1%; a family closely related to the extant South Asian river dolphin), Physeteroidea (2.4%; sperm whales), and to the genus *Chilcacetus* (2.4%; an extinct lineage of homodont, long-snouted dolphins) (Fig. 6B).

Kentriodontids belong to an undescribed species within the genus *Kentriodon* Kellogg, 1927. This kentriodontid is the most common cetacean taxon at Ullujaya, being known by several crania, some of which are associated with mandibles and partial postcranial. Seven of these crania (MUSM 586, 631, 1393, 1397, 1398, and 2431) have been collected and are now under study. Squalodelphinid remains include: 1) two specimens of *Huaridelphis raimondii* (the holotype MUSM 1396,

246 consisting of an isolated cranium, and the referred specimen MUSM 1403, a cranium, fragmentary
247 mandible and some associated postcranial bones) (Lambert et al., 2014); 2) a well-preserved
248 specimen attributed to *Notocetus vanbenedeni* (MUSM 1395, consisting of a cranium with an
249 associated cervical vertebra) (Bianucci et al., 2015); and 3) two indeterminate specimens consisting
250 of a disarticulated partial skeleton (MUSM 1484) and an isolated tympanic bulla (MUSM 1485).
251 Physeteroids consist of two isolated crania: 1) MUSM 3246, referred to cf. *Diaphorocetus* sp.,
252 sharing some affinities with *Diaphorocetus poucheti* from the lower Miocene Monte León
253 Formation of Argentina; and 2) one badly damaged specimen previously regarded as an
254 indeterminate mysticete (Lambert et al., 2014, Bianucci et al., 2015) but now confidently identified
255 as a sperm whale (Physeteroidea indet.). Finally, the long-snouted archaic odontocete *Chilcacetus*
256 *cavirhinus* is represented by two partial skeletons: 1) MUSM 1401, described by Lambert et al.
257 (2015b); and 2) MUSM 2527, currently under study.
258 More than one thousand isolated elasmobranch teeth and spines, representative of at least nine
259 families and sixteen different species, have been collected (Table 2 and Fig. 7). These remains
260 belong to the following four orders: *i*) Carcharhiniformes (57.1% of the specimen), Lamniformes
261 (35.2%), Myliobatiformes (7.5%), and Rhinopristiformes (0.2%) (Fig. 6C).
262 Carcharhiniformes are represented by seven species (*Carcharhinus brachyurus*, *Carcharhinus* cf.
263 *leucas*, *Galeocerdo aduncus*, *Hemipristis serra*, *Negaprion brevirostris*, *Physogaleus contortus*, and
264 *Sphyrna zygaena*), Lamniformes by seven (*Alopias superciliosus*, *Anotodus agassizii*, *Carcharias*
265 sp., *Carcharocles chubutensis*, *Cosmopolitodus hastalis*, *Isurus oxyrinchus*, and *Megalolamna*
266 *paradoxodon*), Myliobatiformes by one or more (Myliobatoidea indet.), and Rhinopristiformes by
267 one (*Anoxypristis* sp.). Almost half of the elasmobranch remains consist of teeth of *C. brachyurus*
268 (49.4%); teeth of *C. hastalis* (22.2%) and *I. oxyrhincus* (8.1%) follow in order of decreasing
269 abundance.
270 Bony fish are represented by an indeterminate cranium, some very fragmentary tuna-like

skeletons, and the partial postcranial of a large istiophorid billfish tentatively referred to aff. *Makaira* sp. Similarly to the Pisco Formation (Collareta et al., 2015; Di Celma et al., 2017), cycloid scales consistent with those of the extant Pacific pilchard *Sardinops* are rather common in *Ct1a*.

Other marine vertebrates include a large dermochelyid marine turtle, represented by a single specimen consisting of some postcranial bones.

4.3. Distribution of the fossil vertebrates

Most of the fossils of vertebrates of Ullujaya come from a 1 km^2-surface area where the *Ct1a* is exposed (Fig. 2A); in turn, based on our field observations, both *Ct1b* and the Ct2 allomember of the Chilcatay Formation exposed in the study area seem devoid of vertebrate specimens preserved as bony elements. Vertebrate fossils have been found between 9.7 and 33.5 m abs, representing a significant portion of the 35 m-thick *Ct1a* (Fig. 6A). Seventy-four specimens (97 % of those with a stratigraphical collocation) are restricted in a 16.9 m-thick interval of sediments (13.9 to 30.8 m abs). The largest concentrations of fossil vertebrate remains are found between 14 and 15 m abs (22 specimens, 29%) and from 25 to 31 m abs (36 specimens, 7%). The large majority of the chondrichthyan specimens was collected from a single fossiliferous interval located about 23 m abs, whereas a few additional remains (mostly referable to *Cosmopolitodus* and *Carcharocles*) come from different horizons within *Ct1a*. Bony fish are homogeneously distributed between 14.2 m and 29.2 m abs, whereas the dermochelyid turtle specimen was found 14.8 m abs.

4.4. Physical taphonomy

Excluding twelve specimens that were not found *in situ* (due to recent erosion and subsequent dislocation), all the fossil vertebrate skeletons whose stratigraphic collocation is known display various degrees of disarticulation and are incomplete (Table 1 and Figs. 8, 9). The associated bones of the disarticulated skeletons exhibit a random disposition without any preferential orientation.

296 Among the sixteen cetacean crania found *in situ*, nine (56.2%) are disposed dorsal side-up and
297 seven (43.8%) are disposed ventral side-up position (Fig. 8A). For most of the studied specimens,
298 all skeletal elements are found within a single sediment layer, and evidence of sinking into the
299 substratum are generally absent. Disarticulated vertebrae are typically observed with their
300 epiphyseal surfaces parallel to the subjacent stratification – a disposition that would prove very
301 stable for a vertebra resting for a prolonged time on a relatively compact soft substrate which does
302 not allow sinking (Figs. 8B-E). The few exceptions include disarticulated vertebrae with transverse
303 processes stuck into the underlying sediment (Figs. 9F, G) and a partly articulated vertebral column
304 that moderately sank into the substratum (Figs. 9H, I).
305 Considering all the cetacean specimens that were found *in situ*, twenty-five of them (48.1%)
306 consist of just one isolated anatomical element (e.g., cranium, vertebra, rib; Fig. 8A), thirteen
307 (25.0%) of a few fully disarticulated bones (ca 25% of the skeleton being preserved; Figs. 8B-E),
308 eleven (21.2%) of a few partially articulated bones (e.g., a few articulated vertebrae and ribs, with
309 the remaining bones being disarticulated; Figs. 8F, G), two (3.8%) of fully disarticulated partial
310 skeletons (ca 50% of the skeleton being preserved; Figs. 8H, I), and one (1.9%) of a fully
311 articulated small portion of the skeleton (seven vertebrae; Figs. 8J, K). The articulation *vs*
312 completeness bivariate bubble plot obtained with the above data (Fig. 10) highlights the high
313 number of specimens whose completeness and articulation equal to zero. As a consequence, the T
314 value is also very low (0.30), thus supporting biostratinomic conditions and processes favouring the
315 disarticulation of the carcasses and the dispersal of the bony elements. The low value (0.08) of r^2
316 and the moderate (0.47) value of rs indicate that articulation and completeness are not firmly related
317 to each other, as also evidenced by the observation of fully disarticulated skeleton with different
318 degree of completeness.
319 Out of the thirteen cetacean skulls collected for systematic study, only one of them retains the
320 mandible (but only the right ramus) articulated, only one has both periotics (ear bones) articulated,

one displays all the teeth in anatomical position, and six lack all teeth in their alveoli.

The smaller sample of non-mammalian vertebrates preserved as skeletal elements (one sea turtle and ten bony fish) confirms the taphonomic pattern observed for the cetaceans, all the detected skeletons being more or less incomplete and articulated. In particular, among bony fish, the most complete specimen (referred to aff. *Makaira* sp.) consists of an articulated, significant portion of the vertebral column with several skeletal elements scattered in a few square metres. The other fish specimens consist of six isolated portions of partly articulated vertebral columns (Figs. 9D, E), one fully articulated caudal fin (Fig. 9C), one isolated cranium, and two fragmentary portions of skulls.

Molluscs, barnacles, worm tubes, and other invertebrate remains, as well as shark teeth, are never found strictly associated to the bones. Bioerosion due to macro-invertebrates is never observed on the fossil bones, whereas shark bite marks are occasionally encountered (see paragraph 4.5). Bioturbations caused by the bone-eating worm *Osedax* (Kiel et al., 2010) and other evidences of whale fall communities (Smith et al., 2015) have not been observed. None of the detected specimens was found included and/or associated to carbonate concretions, unlike what has been observed in the overlying Pisco Formation (Gariboldi et al., 2015; Gioncada et al., 2016). Furthermore, macroscopic evidence of adhering phosphate crusts or envelopes has not been observed.

Macroscopically, most of the bones preserved within the sediment have a reddish colour and appear well mineralised. SEM-BSE observations on representative samples (Table 3) indicate that the bone tissue is rather dense (Figs. 11A, B), confirming a good degree of mineralisation, with well-preserved bone structures. Under the optical microscope, in both the compact and the cancellous bone, Haversian canals and medullary cavities may exhibit cementation (Table 3 and Figs. 11C-F). In one of the samples, Ca-phosphate partially fills osteon porosity, indicating incipient permineralisation. In several cases (Table 3), the Haversian canals of the compact bone and the larger medullary cavities of the cancellous bone are totally or partially filled by Ca-Mg carbonates.

346 Several generations of carbonate cement are observed, having different Ca/Mg ratios. Furthermore,
347 in several samples, sediment grains fill some of the bone cavities, thus providing evidence that the
348 bone went broken before diagenesis occurred. In some cases, Fe-oxides/hydroxides fill the
349 Haversian canals in the reddish portions of the bone. Gypsum can also fill partly the bone cavities.
350 When the external part of the bone is preserved, it can be intact, partly dissolved, or affected by
351 microborings. Two of the four examined specimens having bones not decorticated exhibit
352 microborings of the B-type (*sensu* Gariboldi et al., 2015) (Table 3). In these cases, borings are a few
353 μm wide and can be filled by gypsum, apatite, or Fe-oxyhydroxides. The boundary between the
354 bone tissue and the sediment is cemented by Fe-oxyhydroxides causing the bone surface to appear
355 reddish.
356 Field evidence of abrasion and fracturing of the exposed bones is often not easy to interpret due
357 to the erosion in the present-day desert. In this respect, the analysis of thirteen partial skeletons
358 collected for systematic study has proven more useful. Most of these fossils lack evidence of
359 abrasion, having their cortical bone well preserved (e.g., the *Chilcacetus cavirhinus* MUSM 1401
360 and the *Huaridelphis raimondii* MUSM 1403). However, weak abrasion is observed in some crania
361 of the MUSM collections (e.g., the *Kentriodon* MUSM 2431 and MUSM 631), but that could be
362 due to recent erosion. Fracturing is clearly observed in one cranium (MUSM 631) referred to
363 *Kentriodon*, having its posterior portion damaged (Figs. 12A, B). In all the other collected skulls,
364 fractures (if present) are minor and do not generate significant distorsion of the bones (e.g., in the
365 holotype skull MUSM 1396 of *Huaridelphis raimondii*, Figs. 12C, D). Delicate bone elements,
366 such as the hamular processes and the laminae of the pterygoid, are preserved in several crania.
367 With regard to the postcranial remains, most bones are broken and fragmentary (in part, because of
368 recent erosion), although some vertebrae exhibit a good state of preservation of the narrow and
369 elongated neural spine and transverse processes.
370

371 *4.5. Shark bite marks*

372 Although shark bite marks were not observed in the field on the exposed surfaces of bones, four
373 of the specimens collected for systematic study are affected by these traces (Fig. 13).

374 Only one of the eleven collected crania exhibits bite marks. It consists of an isolated cranium
375 referred to *Kentriodon* sp. (MUSM 1398) displaying two unserrated marks on the dorsal surface of
376 the right premaxilla at mid-length of the rostrum (Fig. 13O). Considering that these traces are short
377 (*ca* 5 mm long) and shallow, they are probably due to scavenging rather than to active predation.
378 This hypothesis is consistent with the feeding behaviour of the extant white shark *Carcharodon*
379 *carcharias*, which usually does not target the head region of dolphins in order to avoid biosonar
380 detection (Long and Jones, 1996).

381 Two partial skeletons referred to *Chilcacetus cavirhinus* (MUSM 1401 and MUSM 2527) and
382 one partial skeleton referred to *Huaridelphis raimondii* (MUSM 1403), exhibit bite marks on
383 postcranial bones. Interestingly, to date, these three specimens are the only fossil vertebrates from
384 Ullujaya for which significant postcranial material was collected, suggesting that bite marks could
385 be relatively frequent on the postcranial remains of the Ullujaya odontocetes. The lack of field
386 observations of bite marks could be favoured by the limited exposure of the bones and to the only
387 partial preservation, due to recent erosion, of their cortical region.

388 The partial skeleton of *Chilcacetus cavirhinus* MUSM 2527 exhibits several bite marks on one of
389 the three preserved ribs (Fig. 13A) and on the left humerus (Figs. 13B, C). Considering the
390 unserrated nature and the size of these marks, all the bites observed on MUSM 2527 bones could
391 have been inflicted by a young individual of *Cosmopolitodus hastalis*, a shark species known from
392 *Ct1a* by abundant teeth. The (?)posterior rib is affected by several marks, the longest of which,
393 about 20 mm long, are a type V bite mark (removing of a roughly prismatic or wedge-shaped chip
394 of bone due to ubiquitous biting or as a result of a single cutting action directed deep into the bone;
395 Collareta et al., 2017a) and two parallel type I marks (Cigala Fulgosi, 1990; Bianucci et al., 2010b).

The humerus is affected by two clusters of bite marks on the lateral and medial surfaces of the bone. Both clusters consist of several type I-II-III bite marks exhibiting a preferential orientation orthogonal to the main axis of the humerus, with several marks crossing each other. These marks are moderately deep, with lengths ranging from a few millimetres to 90 mm. They range in shape from rectilinear to weakly arched, their concavity being facing distally. The marks on the medial surface of the humerus are more numerous (ca 30) and generally more elongated than those on its lateral surface (ca 12). Although the skeleton of MUSM 1403 is rather incomplete, some speculations could be made about the trophic interaction between the shark(s) and the dolphin. The traces on the (?)posterior rib suggest an active attack from behind and below, a predation strategy documented for the extant white shark on pinnipeds and dolphins (Long and Jones, 1996; Klimley et al., 1996) and also suggested for other fossil cetaceans whose ribs display bite marks (Cigala Fulgosi, 1990; Bianucci et al. 2010b; Bianucci and Gingerich, 2011). This hypothesis is strengthened by the observation of a large number of marks, some of which are very deep (one even removing a chip of bone), indicating one or more powerful bites possibly causing the death of the dolphin. On the whole, the shape, size, and arrangement of the marks on the humerus suggest that a single shark grasped the flipper of the dolphin, trying to tear it off with repeated bites and by rotating the head (Fig. 13E). The greater number of traces on the medial surface of the humerus could be due to the greater number of functional teeth of the lower jaw of the shark as compared to the upper jaw (Fig. 13D), supposing that the dolphin was in a ventral up position. The pectoral fins are not included among the parts of the body of dolphins targeted by white sharks in active predation events (Long and Jones, 1996) suggesting that the bites on the humerus of MUSM 1403 were inflicted to the agonizing or even dead dolphin after a first attack to the abdomen (Figs. 13F, G). As young white sharks do not generally attack healthy cetaceans, and adult great whites only actively prey upon distinctly smaller food items (Long and Jones, 1996), it is possible that the odontocete individual MUSM 1403 was already weakened when the attack took place. However, as

421 in all documented cases of shark bite marks on fossil cetacean bones (Deméré and Cerutti, 1982;
422 Cigala Fulgosi, 1990; Lambert and Gigase, 2007; Noriega et al., 2007; Ehret et al, 2009; Bianucci et
423 al. 2010b; Bianucci and Gingerich, 2011; Collareta et al., 2017a), it is not easy to discriminate
424 between marks being the result of active predation and marks resulting from scavenging on a
425 carcass, either drifting at the water surface or lying along the seafloor.
426 The other partial skeleton of *Chilcacetus cavirhinus* (MUSM 1401) exhibits bite marks along the
427 left mandible (Fig. 13H) and on the three preserved ribs (Figs. 13I-L). The marks on the left
428 mandible are located on the lateral side of the symphyseal portion and consist of seven 4–7 mm-
429 long unserrated incisions, six of which are type I bites inflicted almost perpendicular to the main
430 axis of the bone, whereas another mark is a type V mark. Both the (?)second ribs are deeply incised
431 with several bite marks. The (?)second left rib is almost complete and exhibits a high concentration
432 of traces on its proximal posterior surface, where two deep, parallel, unserrated, *ca* 15-mm-long
433 type I marks are observed alongside one irregular hole referable to the vertical impact of a shark
434 tooth. The other marks are smaller and include a type III mark with parallel incisions produced by a
435 serrated tooth. The longest traces on the fragmentary (?)second right rib are: 1) two (type II?)
436 marks, 21 and 13 mm long respectively, on the proximal posterior surface of the bone, and 2) a type
437 I or II mark, 16 mm long, on its anteroventral surface. The third incomplete rib exhibits some small
438 type I marks on the dorsal surface and some weak incisions on the neck of the missing tubercle. The
439 few long and deep unserrated marks detected on this bone, closely associated to several small and
440 shallower traces (including one with serrated margins), suggest that the dolphin was first attacked or
441 scavenged by one or more large lamniform sharks with non-denticulated teeth (e.g.,
442 *Cosmopolitodus*), then by smaller sharks (belonging to at least two different species) scavenging
443 preferentially those parts of the carcass that were previously lacerated by stronger bites. Scavenging
444 on cetaceans killed by other sharks is well documented in present-day mackerel sharks (Pratt et al.,
445 1982; Casey and Pratt, 1985; Long and Jones, 1996).

Finally, the *Huaridelphis raimondii* partial skeleton MUSM 1403 exhibits some shallow incisions (most likely due to scavenging) near the end of a rib fragment (Fig. 13M) and two deep and short type I bite marks on the dorsal margin of another proximal rib fragment (Fig. 13N).

5. Discussion

5.1. Reconstruction of the depositional environment

Facies architecture, bedding patterns, and skeletal composition of the *Ct1b* clinoforms described here bear striking similarities with seaward-prograding mixed siliciclastic-carbonate wedges documented by Pomar and Tropeano (2001) and Massari and D'Alessandro (2012) and reflect the outwards dispersal of sediment in concert with the skeletal production rate and the available physical accommodation space (*sensu* Pomar and Kendall, 2008). According to these interpretations, *Ct1b* represents an entirely Submerged Infralittoral Prograding Wedge (ILPW; Hernández-Molina et al., 2000; Pomar et al., 2015), characterised by a storm-wave-graded profile, located at shoreface depth between the fair-weather and storm wave base, and distinctive clinoform foresets (Fig. 14). In this setting, high wave-current shear-stress in shoreface environment ensures that topsets of subaqueous clinoforms are regions of dominant sediment bypass through lateral advection, erosion, and redistribution. Accordingly, it is inferred that coarse-grained skeletal hash derived from a shallow-water carbonate factory inboard of the clinoform break-points was occasionally transported seawards and deposited on the sloping front of the ILPW separating the shoreface and the offshore (transition-slope setting of Pomar and Tropeano, 2001), leading to the formation of the clinoform foresets.

Downdip transport and dispersion of skeletal debris were especially active during storms by downwelling currents transforming into gravity flows at the clinoformed slope margin (Massari and Chiocci, 2006). At the same time, the winnowed-out fine-grained material actively bypassed the ILPW as part of the suspended load and was deposited farther downdip, into a deeper inner shelf

environment.

Basinward, these clinoformed skeletal-rich sediments interfinger with and downlap onto the vertebrate fossil-bearing siltstones and fine-grained sandstones of *Ct1a*. Given its downdip position with respect to the ILPW, *Ct1a* is considered to represent deposition by suspension fallout of shoreface-derived fine-grained material. The sharp-based, granule- to cobble-sized conglomerate beds interbedded into these fine-grained background sediments clearly reflect periodic high-energy events in otherwise quite marine offshore settings. Accordingly, they are interpreted as event beds resulting from tsunami backflows or storm-induced, offshore-directed density underflows transporting coarse-grained shoreface sediments beyond the toe of the transition slope. The exclusive association of discrete burrowed intervals with gravity-flow event beds intercalated in otherwise poorly bioturbated sediments and the restriction of burrow assemblages to *Thalassinoides* and *Gyrolithes* ichnogenera suggest a genetic relationship between bioturbation by decapod crustaceans and gravity flow deposition. As such, the *Thalassinoides*-*Gyrolithes*-burrowed intervals documented within *Ct1a* resemble the “doomed pioneers trace fossil assemblages” documented by Föllmi and Grimm (1990). In their doomed pioneer hypothesis, the authors argued that ichnofabrics beneath gravity-flow event beds deposited in generally inhospitable environments (e.g., benthic oxygen-deficiency) may be the product of adult allochtonous crustaceans that probably grew up in the well-oxygenated marginal areas and survived exhumation, transport by gravity-driven sediment flows, and re-deposition into deeper-water, oxygen-depleted depositional sites. Based on their interpretation, the displaced callianassid tracemakers are versatile enough to live and feed under the new oxygen-deficient bottom conditions for a short period of time before dying from suffocation and, therefore, may successfully penetrate the substrate to create conspicuous dwelling burrow networks. Accordingly, the systematic absence of additional ichnogenera and autochthonous body fossils of shelled benthic organisms throughout *Ct1a* supports the possibility that the *Thalassinoides*-*Gyrolithes*-burrowed intervals reflect short-term burrowing activity of doomed

pioneers in an otherwise oxygen-deficient sea-bottom environment normally inhibiting benthic life (Föllmi and Grimm, 1990).

Further supporting the hypothesis of poorly oxygenated bottom waters, we observed the presence of disseminated iron oxide framboids, which we interpret as relics of pyrite framboids, in the sediments of *Ct1a*. According to Agbi et al. (2015), the size distribution of framboidal pyrite could be used for distinguishing between oxic-dysoxic and euxinic conditions in the palaeo-bottom water, using the method applied by Wilkin et al. (1996) in modern sediments. Wilkin et al. (1996) noticed that pyrite framboids from euxinic environments are generally smaller and less variable in size than those from sediments underlying oxic or dysoxic bottom water, and related this feature with the different formation mechanisms of pyrite (Raiswell and Berner, 1985), which is syngenetic in euxinic settings and diagenetic in sediments underlying oxic water columns. In the *Ct1a* sediments exposed at Ullujaya, the size distribution of ex-pyrite framboids suggests an alternation of periods characterised by euxinic and oxic-dysoxic conditions (Figs. 5, 15). As recorded in the modern euxinic environments (Wilkin et al., 1996), framboids from samples UL-D1, UL-D2, UJA-49, and UL-D5 exhibit a mean diameter close to 5.0 ± 1.7 μm and large (i.e., > 10 μm) framboids are scarce, accounting for less than 4% of the measured aggregates. Indeed, framboids from sample UL-D3 exhibit a mean diameter of 8.3 μm (± 4.8) and more than 30% of them is large-sized, in agreement with the description of pyrite aggregates from modern oxic-dysoxic environments, with a mean of 7.7 ± 4.1 μm and 10-50 % of framboids > 10 μm (Wilkin et al. 1996). Therefore, the *Ct1a* palaeoenvironment of Ullujaya was interested by some euxinic events; on the other hand, the marine fossil assemblages found in the Ct1 allomember, including bivalves and barnacles in the shallow-water *Ct1b* and fish and cetaceans in the inner shelf *Ct1a*, suggest normal oxygenation in nearshore areas, where breaking waves efficiently mixed oxygen from the atmosphere into the water.

A key role in the development of oxygen-deficient conditions on the sea floor was probably

played by local factors, such as the semi-enclosed nature of the EPB during deposition of the Chilcatay strata (Fig. 1B) and the likely presence of a nearby upwelling zone where deep, nutrient-enriched water raised towards the surface, causing increased organic productivity and high oxygen demand on the shelf, as observed along the present-day Eastern Pacific margin (Pickering et al., 1989). As a matter of fact, however, diatom forms that are typical of upwelling settings (e.g., *Thalassionema*) do not occur in Ct1, but they are present in the overlying deposits of the Ct2 allomember.

The record of silicoflagellates from Ullujaya helps in further refining our reconstruction of the depositional environment. The silicoflagellate assemblage from *Ct1a* features the temperate genus *Distephanopsis*, the warm-water genera *Corbisema* and *Naviculopsis*, and the cold-water genus *Stephanocha*. This assemblage is best interpretable as witnessing warm-temperate thermal conditions.

Finally, an approximate estimation of the palaeobathymetry recorded by the toe of the slope at the transition between *Ct1a* and *Ct1b* can be obtained by summing up the depth of the break-points of the clinobedded units and the thickness of the clinobeds (15-20 m in *Ct1b*). The outer edge of the infralittoral wedge is naturally dependent on many different environmental factors, of which the wave climate, fetch, grain size, and general oceanographic conditions are among the most important (Mitchell et al., 2012). In the Mediterranean area, both Hernández-Molina et al. (2000) and Massari and Chiocci (2006) have found the outer edges of the breakpoints of the clinobedded units located at water depths of about 15–20 m. Due to the protected palaeogeography displayed by the EPB (Fig. 1B), the hydrodynamic conditions during deposition of the Chilcatay Formation would have been remarkably less energetic from those dictating the development of modern non-tropical skeletal carbonate sediments in oceanic settings exposed to vigorous storm-waves and probably resulted in the formation of prograding wedges at relatively shallower water depths. As a consequence, by assuming a water depth of the outer edge of the infralittoral wedge similar to that documented in the

546 Mediterranean area, an offshore depositional setting at least 30-40 m below the sea level can be
547 interpreted for *Ct1a* at the toe of the slope.
548 The bioturbated nature of the lower boundary of the Ct2 allomember and its association with a
549 basal oyster-bearing shelly horizon and a mixture of extrabasinal pebble- to boulder-size clasts,
550 indicate that erosional scouring and shell concentration took place during a period of sea-level fall
551 followed by transgression (e.g., Kidwell, 1991; Abbott, 1998; Carnevale et al., 2011).
552
553 *5.2. Genesis of the marine vertebrate fossil assemblage*
554 Our taphonomic observations and the reconstruction of the *Ct1a* depositional environment
555 suggest prolonged flotation and repeated movements through the water mass of the marine
556 vertebrate carcasses before their final deposition on the seafloor (Schäfer, 1972). During this long-
557 time floating phase, the carcasses were subject to biogenic and physical processes of partial
558 destruction, as supported by the shark bite marks (at least part of them indicating scavenging action)
559 and by the overall low degrees of completeness and articulation of the specimens. The high number
560 of isolated crania of cetaceans may record the separation of the relatively heavy head from the rest
561 of the body during the early phases of the flotation of the carcasses, as observed by Schäfer (1972)
562 for extant dolphins and already hypothesised for fossil cetaceans from the upper Miocene of the
563 EPB by Bianucci et al. (2010a). Further disarticulation could have occurred during the period when
564 the carcasses laid exposed on the seafloor, due to the fluidization of the remaining soft tissues and
565 consequent gravitational collapse (Reisdorf et al., 2014). In some cases, the presence of sediment
566 infilling some bone cavities proves that the micro-breakages of the bones occurred before
567 diagenesis and that bones were exposed on the seafloor after the carcass deposition, as a
568 consequence of the early body dismemberment.
569 Bottom currents can be discarded as a cause of disarticulation due to the lack of preferential
570 orientation of the disarticulated remains and the lack of sedimentary structures, considering also that

571 the aforementioned evidence of euxinic conditions supports water stagnation close to the seafloor.
572 Together with the scarcity of breakage and abrasion marks on the bones, the preservation of delicate
573 bone structures further supports the absence of transport due to bottom currents. Scavenging action
574 as a cause of disarticulation can be discarded due to the lack of fossil traces on the bones (with the
575 notable exception of those left by sharks) and of closely associated macroinvertebrate remains
576 (whose absence is probably due to the euxinic conditions of the bottom waters, see above).
577 Bones often exhibit a reddish colour on the surface, visible at both macro- and micro-scale (Figs.
578 11C-F and 13). This feature is probably due to the oxidation of Fe, available for the formation of
579 abundant pyrite framboids in anoxic bottom water and within the sediments.
580 Bone cavities, such as Haversian canals and medullary cavities, show in some cases a Ca-
581 phosphate filling that occurred during early diagenesis and a later cementation of carbonates (spatic
582 calcite and subordinate Mg-Ca carbonates) or gypsum. Differing from what has been recorded at
583 various sites of the Pisco Formation, micritic clotted dolomite filling the bone cavities and dolomite
584 envelopes have not been observed with fossil vertebrates at Ullujaya. In the deposits of the Pisco
585 Formation, dolomite concretions grew around vertebrate carcasses during the very early phases of
586 diagenesis, as a consequence of anaerobic degradation processes of organic matter leading to
587 cementation of the surrounding matrix (Gariboldi et al., 2015; Gioncada et al., 2016, 2018).
588 Therefore, the formation of dolomite nodules requires an early covering of the vertebrate carcass by
589 sediment (e.g., via sinking into a soupy substrate or rapid burial by high rates of sediment
590 deposition) (Gariboldi et al., 2015; Gioncada et al., 2016). Moreover, microbially mediated
591 degradation processes inducing dolomite precipitation are more likely to be efficient if the amount
592 of decaying organic matter is large and permeability of the embedding sediment is low, both
593 conditions favouring a locally anoxic environment (Gioncada et al., 2018). At Ullujaya, taphonomic
594 and sedimentological evidence accounts against rapid sinking and/or burial of the vertebrate
595 carcasses, supporting instead the hypothesis that their deposition occurred after substantial

596 defleshing and the consequent exposure of the bones on the seafloor. Such a prolonged
597 biostratinomic journey likely contributed to prevent the formation of dolomite envelopes around the
598 Ullujaya marine vertebrate remains.
599 The fine-quality preservation of the bones, the absence of adhering phosphate crusts or nodules,
600 and the above reported sedimentary evidence also exclude the interpretation of the *Ct1a* vertebrate
601 assemblage as a condensed deposit due to hiatal and/or lag concentration consequent to low
602 sedimentation rates or erosion (see Pyenson et al., 2009; Boessenecker et al., 2014).
603
604 *5.3. Stratigraphic significance and comparison with other coeval vertebrate assemblages*
605 *5.3.1. Cetaceans*
606 At the species level, the Ullujaya assemblage shares the squalodelphinid *Notocetus vanbenedeni*
607 with the Aquitanian–lower Burdigalian Leonian assemblage, Argentina (Cozzuol, 1996). Similarly,
608 both faunas include a species of *Kentriodon*, and a physeteroid from Ullujaya displays similarities
609 with the Leonian *Diaphorocetus poucheti*. A squalodelphinid and a physeteroid are also recorded in
610 the upper Aquitanian-lower Burdigalian Belluno assemblage, Italy (Bianucci and Landini, 2002),
611 whereas at least one squalodelphinid and *Kentriodon* are known from the lower Miocene formations
612 of the eastern U.S.A (Kellogg, 1932; Whitmore and Kaltenbach, 2008; Kidwell et al., 2015;
613 Boessenecker, 2018). Finally, the long-snouted homodont odontocete *Chilcacetus cavirhinus* may
614 belong to the same clade as the Leonian *Argyrocetus patagonicus* and several species from the
615 Aquitanian Pyramid Hill assemblage, California, U.S.A. (Lambert et al., 2015b).
616 Interestingly, the Ullujaya assemblage features no mysticetes, a condition shared by all other
617 coeval sites, a main exception being the Leonian assemblage, which includes one 'cetothere' and
618 one balaenid (Buono et al., 2017). The Aquitanian gap in the mysticete fossil record could partly
619 reflect a limited number of cetacean-bearing localities (Marx and Fordyce, 2015). The low diversity
620 of early Miocene filter-feeding mysticetes may also be correlated to a drop in diatom diversity that

621 would have particularly impacted cetaceans preying upon small-sized prey (Marx and Uhen, 2010).
622 The fact that the Argentinian localities are the southernmost among these lower Miocene
623 assemblages may suggest that the circum-Antarctic areas were refuge regions for mysticetes at that
624 time.
625 *5.3.2 Elasmobranchs*
626 Many elasmobranch taxa found at Ullujaya are stratigraphically uninformative, being common
627 components of Neogene chondrichthyan assemblages from shallow-marine settings worldwide.
628 Most of them are also known from the late Miocene deposits of the EPB (Di Celma et al., 2017;
629 Landini et al., 2017a). However, two otodontid taxa (*Megalolamna paradoxodon* and *Carcharocles*
630 *chubutensis*) are of particular stratigraphic interest. *M. paradoxodon* is known from a few localities
631 worldwide, being seemingly limited to the Aquitanian–Burdigalian interval (Shimada et al., 2017).
632 In turn, *Carcharocles* is one of the most ubiquitous and widespread Neogene elasmobranch genera.
633 Pimiento et al. (2016) suggested that *Carcharocles* represents a lineage of chronospecies whose
634 latest representatives are *C. chubutensis* (making its last appearance in Oligocene or earliest
635 Miocene times) and the late early Miocene–Pliocene *C. megalodon* (whose presence in Burdigalian
636 deposits has been demonstrated by Carrillo-Briceño et al., 2015). The present report of remains of
637 *C. chubutensis* (including fragmentary adult teeth, always displaying lateral cusplets) from Ullujaya
638 could suggest that *C. chubutensis* and *C. megalodon* coexisted during the late early Miocene (see
639 also Aguilera and Aguilera, 2004). On the other hand, *C. chubutensis* and *C. megalodon* are not
640 found together in the EPB, as *C. megalodon* is absent from the Chilcatay Formation, being in turn
641 the sole otodontid featured in the geologically younger Pisco Formation (Landini et al., 2018).
642 *5.3.3 Bony fish*
643 Both the family Istiophoridae and the scombrid genus *Thunnus* are known from the Eocene
644 onwards (Fierstine, 2006; Santini et al., 2013). Fossil pilchards are very rare in the Pacific realm,
645 and the origin itself of the genus *Sardinops* is only tentatively referred to the early Miocene (Parrish

et al., 1989). Tuna-like fish, marlins, and *Sardinops* are also known from the upper Miocene strata of the EPB (Collareta et al., 2015, 2017b; Lambert et al., 2015a; Bianucci et al., 2016a; Di Celma et al., 2017).

5.3.4 Turtles

The fossil history of dermochelyids spans from the Palaeocene onwards (Delfino et al., 2013). A dermochelyid turtle (*Natemys peruvianus*) has been described based on a partial shell from the "Late Oligocene Pisco Formation […] approximately 1.5 km southwest of Hacienda Ullujaya" (Wood et al., 1996). Based on our observations, only the Chilcatay Formation is exposed at that locality; that would also account better for the proposed Oligocene age of *Natemys peruvianus*.

5.4. Vertebrate palaeoecology

5.4.1. Cetaceans

Palaeoecological analyses of fossil cetacean assemblages must account for some major caveats. First, floating cetacean carcasses can suffer substantial transport by marine or fluvial currents before depositing at the seafloor (Schäfer, 1972). Second, the reconstruction of the feeding and habitat preferences of fossil cetaceans is not obvious when the fossil taxa do not have close and phenetically similar extant relatives (e.g., *Chilcacetus* and cf. *Diaphorocetus*). Third, the absence of some significant clades of large-sized cetaceans (e.g., mysticetes) could reflect long-term biogeographical patterns rather than eco-environmental constraints. Finally, some of the Ullujaya fossil cetaceans could have entered accidentally, as living organisms, into the sheltered *Ct1a* area from adjacent fluvial or pelagic environments. Given these limitations, the reconstructed scenario of Figure 14 should be regarded as partly speculative. However, we are confident that at least the small dolphin *Kentriodon*, the most common cetacean in *Ct1a*, likely lived in this area.

Most of the Ullujaya cetaceans (*Chilcacetus*, *Huaridelphis*, *Kentriodon*, and *Notocetus*) exhibit narrow rostra and small teeth; moreover, they are homodont and polydont, thus suggesting a

raptorial feeding specialization for capturing small prey (e.g., small-sized fish and shrimps). Taphonomic selection, preventing the preservation of the delicate skeletons of small-sized vertebrates and decapods, could account for the apparent lack of fossils of these hypothetical prey items at Ullujaya. Given its very elongated and narrow rostrum and symphyseal portion of the mandibles, *Chilcacetus cavirhinus* could have been a coastal bottom-feeder (as the extant river dolphins) or an epipelagic piscivore (as hypothesised for the similarly long-snouted late Miocene beaked whale *Messapicetus gregarius*: Lambert et al., 2015a; Ramassamy et al., 2018). In both hypotheses, the long-snouted condition could have been driven by dietary preferences (e.g., a predilection for small fish) rather than by environmental conditions (McCurry et al., 2017).

The physeteroid cranium referred to cf. *Diaphorocetus* displays deep dental alveoli indicating a complete upper dentition and evoking a raptorial feeding behaviour that contrasts with the suction feeding technique of extant sperm whales. Compared to the size of the skull, the diameter of the alveoli is small, suggesting that this odontocete fed on smaller prey than other macroraptorial physeteroids (e.g., the large-toothed *Acrophyseter* and *Livyatan*: Lambert et al., 2017).

The Ullujaya vertebrate assemblage does not feature two recently described Chilcatay odontocetes, namely, the possibly suction feeding *Inticetus* (Lambert et al., 2018) and the macroraptorial squalodelphinid *Macrosqualodelphis* (Bianucci et al., 2018). This observation indicates that the morphological and ecological disparity of the Chilcatay cetaceans is greater than that recorded at Ullujaya.

5.4.2. Elasmobranchs

The Ullujaya elasmobranch assemblage is dominated by remains of *Carcharhinus brachyurus*, which currently inhabits warm-temperate waters 0–100 m deep (Compagno, 1984). *Carcharhinus brachyurus* occasionally occurs in brackish and estuarine waters and elects semi-enclosed embayments as nursery grounds (Duffy and Gordon, 2003). A shallow-water environment is also supported by the presence of *Negaprion brevirostris* and *Carcharhinus* cf. *leucas*, two strongly

littoral, tropical-subtropical carcharhinids that thrive in mangrove swamps and river mouths (Compagno, 1984; Compagno and Niem, 1998). Similarly, *Anoxypristis* is a nectobenthic organism that is found in coastal and estuarine warm-water environments (D'Anastasi et al., 2013). In turn, strong connections with the pelagic realm are supported by the presence of *Alopias superciliosus.* All the recognised extant taxa are nevertheless consistent with a coastal environment. A predilection for coastal warm-temperate habitats is also regarded as characteristic of the extinct species *Carcharocles chubutensis*, *Megalolamna paradoxodon*, and *Hemipristis serra*; moreover, the extant *Hemipristis elongata* is a tropical coastal shark that inhabits waters up to 30 m depth (Compagno, 1984). The ontogenetic structure of the observed assemblage also suggests a shallow coastal environment, as *Carcharhinus brachyurus* and *Cosmopolitodus hastalis* are mostly represented by juvenile teeth, thus evoking the presence of overlapping coastal nurseries (e.g., Landini et al., 2017b, 2018). *Alopias superciliosus*, *Carcharhinus brachyurus*, *Isurus oxyrinchus*, *Negaprion brevirostris*, and *Sphyrna zygaena* mostly rely on small- to medium-sized fish and subordinate cephalopods and crustaceans, and similar considerations apply to the extant species of *Carcharias* and *Hemipristis* (Compagno, 1984, 2001; Cortés and Gruber, 1990; Devadoss and Chandrasekar, 1991; Smale, 1991; Duffy and Gordon, 2003; Manojkumar and Pavithran, 2004; Cailliet et al., 2009). In turn, the more diverse trophic habits of *Carcharhinus leucas* and extant *Galeocerdo* include occasional predation upon marine tetrapods (including diminutive cetaceans) (Simpfendorfer and Burgess, 2009). *Anotodus agassizii* and *Cosmopolitodus hastalis* have been interpreted as eurytrophic littoral predators whose adult stages foraged mostly on fish while secondarily preying on diminutive marine tetrapods (e.g., Landini et al., 2017a). Among Otodontidae, *Megalolamna* is regarded as a piscivore which relied on medium-sized fish (Shimada et al., 2017), whereas the diet of *Carcharocles* was likely similar to that of extant *Carcharodon* – i.e., characterised by a high contribution of marine mammals (Collareta et al., 2017a).

As reported above, shark bite marks have been detected on some odontocete bones from

721 Ullujaya. These bones are referable to cetaceans roughly ranging in size between 1.5 m
722 (*Kentriodon*) and 3.2 m (*Chilcacetus*). This size range overlaps with that of the known cetacean
723 prey of large individuals of extant white sharks (e.g., Long and Jones, 1996). The bite marks are
724 mostly referable to sharks with unserrated teeth. Smooth-edged teeth of *C. hastalis* are among the
725 most common fossils at Ullujaya; this species presumably attained maximum size values
726 comparable to those of the largest extant lamnids (Purdy et al., 2001). It is thus likely that *C.*
727 *hastalis* was the most prominent predator of cetaceans in the Ullujaya palaeoecosystem. However,
728 most of the *C. hastalis* teeth from Ullujaya belong to immature individuals, and juveniles of this
729 species may have focused their diet on fish (Collareta et al., 2017b). Therefore, considering that
730 large teeth referable to full-grown lamniforms (including also *C. hastalis*) are occasionally found all
731 along the studied section, and taking also into account that extant mackerel sharks do not actively
732 prey upon animals from their own size class, the most efficient predators of cetaceans at Ullujaya
733 should have included large, transient individuals of *C. hastalis*. Bites due to scavenging on floating
734 carcasses should also be taken into account, as it is known that large-sized white sharks feature a
735 significant component of cetacean carrion in their diet (Long & Jones, 1996; Fallows et al., 2013).
736 Among rays, forms such as *Myliobatis* and *Anoxypristis* forage mainly on bentho-demersal prey,
737 including hard-shelled invertebrates, fish, and squids (e.g., Jardas et al., 2004; Peverell, 2009:
738 Molina and Cazorla, 2015; Rezende et al., 2015).
739 The Ullujaya elasmobranch assemblage is thus dominated by mesopredators, i.e., by juveniles
740 and adults of species whose mature stages mainly relied on fish and macro-invertebrates and by
741 juveniles of top-predator species (e.g., juveniles of *C. hastalis*) whose adult stages featured a
742 significant component of marine tetrapods in their diet.
743 *5.4.3 Bony fish*
744 The co-occurrence of two families of primarily oceanic bony fish (Istiophoridae and
745 Scombridae) supports connection with the open-ocean environment. Extant marlins are generally

746 close to the apex of pelagic food pyramids (Kitchell et al., 2006), their diet including large-sized
747 bony fish such as mackerels, whereas tuna-like scombrids are opportunistic predators that feed at a
748 slightly lower trophic level (Bertrand et al., 2002). Pilchards are small-sized epipelagic schooling
749 fishes that inhabit highly productive coastal-pelagic environments and may enter semi-enclosed
750 embayments; huge populations of *Sardinops* inhabit the present-day waters off Peru and represent a
751 key prey item for other vertebrates (Chavez et al., 2003). Strong fossil evidence indicates that,
752 during the late Miocene, *Sardinops* occupied a prominent position in the trophic chains of the EPB
753 (Collareta et al., 2015, 2017b; Lambert et al., 2015). Pilchards likely also represented a fundamental
754 trophic link at Ullujaya in Burdigalian times, although they were perhaps more common seawards
755 of the Gran Tablazo Archipelago.

756 *5.4.4 Turtles*

757 The sole extant dermochelyid, *Dermochelys coriacea*, is a strongly pelagic organism that feeds
758 on gelatinous invertebrates (Eckert et al., 2012). A dermochelyid in the semi-enclosed embayment
759 of Ullujaya could suggest the presence of a nesting site in proximity of this area. Indeed, extant
760 dermochelyids elect coarse-grained beaches (sometimes within protected embayments) with little
761 abrasive clasts (e.g., coral fragments), and a steep approach to the sea as nesting sites (COSEWIC,
762 2012).

763

764 **6. Conclusions**

765 We investigated an early Miocene (Burdigalian) vertebrate assemblage dominated by diverse
766 toothed cetaceans and elasmobranchs from the *Ct1a* facies association of the Chilcatay Formation
767 of southern Peru.

768 Based on sedimentological, ichnological, and palaeontological considerations, *Ct1a* represents a
769 sandy-silty sediment wedge deposited in a warm-temperate, 30-40 m in water depth, semi-enclosed
770 embayment, connected with riverine and open-ocean environments and with recurrent euxinic

771 conditions at the seafloor.

772 Vertebrate skeletons are typically disarticulated and incomplete, and some of these are affected
773 by shark bite marks. Bioerosion due to macro-invertebrates is never observed and none of the
774 specimens was found included and/or associated to carbonate concretions.

775 A long-time floating phase allowed biogenic and physical partial destruction of the carcasses
776 before deposition on a soft compact substrate. Oxygen-deficient bottom conditions inhibited the
777 scavenging action of benthic organisms.

778

779 **Acknowledgments and funding**

780 We thank T. J. DeVries, F. G. Marx, K. Post, R. Salas-Gismondi, M. Martínez-Cáceres, V.
781 Pacheco, and J. Tejada for their help during multiple field prospections and several fruitful
782 discussions. Special gratitude to W. Aguirre and E. Díaz, for field assistance and fossil preparation.
783 Thanks also to V. Barberini for the help with the radiometric analyses. Comments and suggestions
784 by T. J. Algeo, R. W. Boessenecker, H. Falcon-Lang, and an anonymous reviewer greatly improved
785 the quality of this work.

786 This study was supported by a grant from the Italian Ministero dell'Istruzione, dell'Università e
787 della Ricerca [PRIN Project, 2012YJSBMK] to G. Bianucci, E. Malinverno, and C. Di Celma, two
788 grants from the National Geographic Society Committee for Research Exploration to G. Bianucci
789 [9410–13] and to O. Lambert [GEFNE177-16], and a grant by the University of Pisa to G. Bianucci
790 [PRA_2017_0032]. Field work by O. Lambert, C. de Muizon, and G. Bianucci in 2010 and 2011
791 was supported by the Action Thématique Muséum (ATM) ‘Etat et structure phylogénétique de la
792 biodiversité actuelle et fossile’ and by the Centre National de la Recherche Scientifique (CNRS),
793 with logistical support of the Institut Français d’Etudes Andines (IFEA) and of the Institut de
794 Recherche pour le Développement (IRD).

795

796 **References**

797 Abbott, S.T. (1998). Transgressive systems tract and onlap shellbeds from mid-Pleistocene
798 sequences, Wanganui Basin, New Zealand. *Journal of Sedimentary Research*, 68, 253-268.
799 Agbi, I., Ozibo, B., Newton, R. (2015). Pyrite framboid size distribution of the Grey Shales
800 (Yorkshire UK) as an indication of redox conditions. *IOSR Journal of Applied Geology and*
801 *Geophysics*, 3, 36-42.
802 Aguilera, O.A., Aguilera, D.R. (2004). Giant-toothed white sharks and wide-toothed mako
803 (Lamnidae) from the Venezuela Neogene: their role in the Caribbean, shallow-water fish
804 assemblage: *Caribbean Journal of Science*, 40, 368-382.
805 Beardmore, S. R., Furrer, H. (2016a). Taphonomic analysis of *Saurichthys* from two stratigraphic
806 horizons in the Middle Triassic of Monte San Giorgio, Switzerland. *Swiss Journal of*
807 *Geosciences*, 109, 1-16.
808 Beardmore, S. R., Furrer, H. (2016b). Evidence of a preservational gradient in the skeletal
809 taphonomy of Ichthyopterygia (Reptilia) from Europe. *Palaeogeography, Palaeoclimatology,*
810 *Palaeoecology*, 443, 131-144.
811 Beardmore, S. R., Orr, P. J., Manzocchi, T., Furrer, H., Johnson, C. (2012). Death, decay and
812 disarticulation: modelling the skeletal taphonomy of marine reptiles demonstrated using
813 *Serpianosaurus* (Reptilia; Sauropterygia). *Palaeogeography, Palaeoclimatology, Palaeoecology*,
814 337, 1-13.
815 Bertrand, A., Bard, F. X., Josse, E. (2002). Tuna food habits related to the micronekton distribution
816 in French Polynesia. *Marine Biology*, 140, 1023-1037.
817 Bianucci, G., Bosio, G., Malinverno, E., Muizon, C. de, Villa, I. M., Urbina, M., Lambert, O.
818 (2018). A new large squalodelphinid (Cetacea, Odontoceti) from Peru sheds light on the Early
819 Miocene platanistoid disparity and ecology. *Royal Society Open Science*, 5, article #172302.
820 Bianucci, G., Di Celma, C., Collareta, A., Landini, W., Post, K., Tinelli, C., Muizon, C. de, Bosio,

821 G., Gariboldi, K., Gioncada, A., Malinverno, E., Cantalamessa, G., Altamirano-Sierra, A., Salas-
822 Gismondi, R., Urbina, M., Lambert, O. (2016a). Fossil marine vertebrates of Cerro Los Quesos:
823 Distribution of cetaceans, seals, crocodiles, seabirds, sharks, and bony fish in a late Miocene
824 locality of the Pisco Basin, Peru. *Journal of Maps*, 12, 1037-1046.
825 Bianucci, G., Di Celma, C., Landini, W., Post, K., Tinelli, C., Muizon, C. de, Gariboldi, K.,
826 Malinverno, E., Cantalamessa, G., Gioncada, A., Collareta, A., Salas-Gismondi, R., Varas-Malca,
827 R.M., Urbina, M., Lambert, O. (2016b). Distribution of fossil marine vertebrates in Cerro
828 Colorado, the type locality of the giant raptorial sperm whale *Livyatan melvillei* (Miocene, Pisco
829 Formation, Peru). *Journal of Maps*, 12, 543-557.
830 Bianucci, G., Gingerich, P.D. (2011). *Aegyptocetus tarfa*, n. gen. et sp. (Mammalia, Cetacea), from
831 the middle Eocene of Egypt: clinorhynchy, olfaction, and hearing in a protocetid whale. *Journal*
832 *of Vertebrate Paleontology*, 31, 1173-1188.
833 Bianucci, G., Lambert, O., Post, K. (2010a). High concentration of long-snouted beaked whales
834 (genus *Messapicetus*) from the Miocene of Peru. *Palaeontology*, 53, 1077-1098.
835 Bianucci, G., Landini, W. (2002). Change in diversity, ecological significance and biogeographical
836 relationships of the Mediterranean Miocene toothed whale fauna. *Geobios*, 35, 19-28.
837 Bianucci, G., Urbina, M., Lambert, O. (2015). A new record of *Notocetus vanbenedeni*
838 (Squalodelphinidae, Odontoceti, Cetacea) from the early Miocene of Peru. *Comptes Rendus*
839 *Palevol*, 14, 5-13.
840 Bianucci, G., Sorce, B., Storai, T., Landini, W. (2010b). Killing in the Pliocene: shark attack on a
841 dolphin from Italy. *Palaeontology*, 53, 457-470.
842 Boessenecker, R. W. (2018). Problematic archaic whale *Phococetus* (Cetacea: Odontoceti) from the
843 Lee Creek Mine, North Carolina, USA, with comments on geochronology of the Pungo River
844 Formation. *PalZ*. doi: 10.1007/s12542-018-0419-3
845 Boessenecker, R.W., Perry, F. A., Schmitt, J. G. (2014). Comparative taphonomy, taphofacies, and

846 bonebeds of the Mio-Pliocene Purisima Formation, Central California: strong physical control on
847 marine vertebrate preservation in shallow marine settings. *PLOS ONE*, 9, article #e91419.
848 Buono, M.R., Fernández, M.S., Cozzuol, M.A., Cuitiño, J.I., Fitzgerald, E.M. (2017). The early
849 Miocene balaenid *Morenocetus parvus* from Patagonia (Argentina) and the evolution of right
850 whales. *PeerJ*, 5, article #e4148.
851 Cailliet, G.M., Cavanagh, R.D., Kulka, D.W., Stevens, J.D., Soldo, A., Clo, S., Macias, D., Baum,
852 J., Kohin, S., Duarte, A., Holtzhausen, J.A., Acuña, E., Amorim, A., Domingo, A. (2009). *Isurus*
853 *oxyrinchus*. In: The IUCN Red List of Threatened Species 2009: e.T39341A10207466.
854 http://www.iucnredlist.org, accessed on April 28, 2018.
855 Carnevale, G., Landini, W., Ragaini, L., Di Celma, C., Cantalamessa, G. (2011). Taphonomic and
856 paleoecological analyses (mollusks and fishes) of the Sua member condensed shellbed, Upper
857 Onzole Formation (early Pliocene, Ecuador). *Palaios*, 26: 160-172.
858 Carrillo-Briceño, J.D., Maxwell, E., Aguilera, O.A., Sánchez, R., Sánchez-Villagra, M.R. (2015).
859 Sawfishes and other elasmobranch assemblages from the Mio-Pliocene of the South Caribbean
860 (Urumaco Sequence, Northwestern Venezuela). *PLOS ONE*, 10, article #e0139230.
861 Casey, J.G., Pratt Jr, H.L. (1985). Distribution of the white shark, *Carcharodon carcharias*, in the
862 western North Atlantic. *Memoirs of the Southern California Academy of Sciences*, 9, 2-14.
863 Chavez, F.P., Ryan, J., Lluch-Cota, S.E., Ñiquen, M. (2003). From anchovies to sardines and back:
864 multidecadal change in the Pacific Ocean. *Science*, 299, 217-221.
865 Cigala Fulgosi, F. (1990). Predation (or possible scavenging) by a great white shark on an extinct
866 species of bottlenosed dolphin in the Italian Pliocene. *Tertiary Research*, 12, 17-36.
867 Clarke, J.A., Ksepka, D.T., Salas-Gismondi, R., Altamirano, A.J., Shawkey, M.D., D'Alba, L.,
868 Vinther, J., DeVries, TJ., Baby, P. (2010). Fossil evidence for evolution of the shape and color of
869 penguin feathers. *Science*, 330, 954-957.
870 Clift, P.D., Pecher, I., Kukowski, N., Hampel, A. (2003). Tectonic erosion of the Peruvian Forearc,

Lima Basin, by steady-state subduction and Nazca Ridge collision. *Tectonics*, 22, article #1023.

Collareta, A., Lambert, O., Landini, W., Di Celma, C., Malinverno, E., Varas-Malca, R., Urbina, M., Bianucci, G. (2017a). Did the giant extinct shark *Carcharocles megalodon* target small prey? Bite marks on marine mammal remains from the late Miocene of Peru. *Palaeogeography, Palaeoclimatology, Palaeoecology*, 469, 84-91.

Collareta, A., Landini, W., Chacaltana, C., Valdivia, W., Altamirano-Sierra, A., Urbina, M., Bianucci, G. (2017b). A well preserved skeleton of the fossil shark *Cosmopolitodus hastalis* from the late Miocene of Peru, featuring fish remains as fossilized stomach contents. *Rivista Italiana di Paleontologia e Stratigrafia*, 123, 11-22.

Collareta, A., Landini, W., Lambert, O., Post, K., Tinelli, C., Di Celma, C., Panetta, D., Tripodi, M., Salvadori, P.A., Caramella, D., Marchi, D., Urbina, M., Bianucci, G. (2015). Piscivory in a Miocene Cetotheriidae: first record of fossilized stomach content for an extinct baleen-bearing whale. *The Science of Nature*, 102, article #70.

Compagno, L.J.V. (1984). FAO Species Catalogue. Vol 4: Sharks of the world, Part 1 - Hexanchiformes to Lamniformes. *FAO Fisheries Synopsis*, 125, 4, 1-250.

Compagno, L.J.V. (2001). Sharks of the world. An annotated and illustrated catalogue of shark species known to date. Volume 2. Bullhead, Mackerel and Carpet Sharks (Heterodontiformes, Lamniformes and Orectolobiformes). FAO, Rome.

Compagno, L.J.V., Niem, V.H. (1998). Carcharhinidae. In: K.E. Carpenter and V.H. Niem (eds.), FAO Identification Guide for Fishery Purposes. The Living Marine Resources of the Western Central Pacific. Food and Agriculture Organization, Rome, 1312-1324.

Cortés, E., Gruber, S.H. (1990). Diet, feeding habits, and estimates of daily ration of young lemon sharks, *Negaprion brevirostris* (Poey). *Copeia*, 1990, 204-218.

COSEWIC [Committee on the Status of Endangered Wildlife in Canada] (2012). COSEWIC assessment and status report on the leatherback sea turtle *Dermochelys coriacea* Atlantic

896 Population Pacific Population in Canada – 2012.https://www.registrelep-
897 sararegistry.gc.ca/default.asp?lang=En&n=9F76DBB0-1, accessed on May 1, 2018.
898 Cozzuol, M. (1996). The record of aquatic mammals in southern South America. *Münchner*
899 *Geowissenchaftliche, Abhandlungen, Rheihe A*, 30, 321-342.
900 D'Anastasi, B., Simpfendorfer, C., van Herwerden, L. (2013). *Anoxypristis cuspidata*. In: The IUCN
901 Red List of Threatened Species 2013: e.T39389A18620409. http://www.iucnredlist.org, accessed
902 on April 28, 2018.
903 Danise, S., Dominici, S. (2014). A record of fossil shallow-water whale falls from Italy. *Lethaia*, 47,
904 229-243.
905 Delfino, M., Scheyer, T. M., Chesi, F., Fletcher, T., Gemel, R., MacDonald, S., Rabi, M., Salisbury,
906 S. W. (2013). Gross morphology and microstructure of type locality ossicles of *Psephophorus*
907 *polygonus* Meyer, 1847 (Testudines, Dermochelyidae). *Geological Magazine*, 150, 767-782.
908 Deméré, T.A., Cerutti, R.A. (1982). A Pliocene shark attack on a cethotheriid whale. *Journal of*
909 *Paleontology*, 56, 1480-1482.
910 Devadoss, P., Chandrasekhar, S. (1991). A note on the rare snaggle tooth shark, *Hemipristis*
911 *elongatus*. *Marine Fisheries Information Service, Technical and Extension Series*, 114, 36.
912 DeVries, T.J. (1998). Oligocene deposition and Cenozoic sequence boundaries in the Pisco Basin.
913 *Journal of South American Earth Sciences*, 11, 217-231.
914 DeVries, T.J. (2017). Eocene stratigraphy and depositional history near Puerto Caballas (East Pisco
915 Basin, Peru). *Boletín de la Sociedad Geológica del Perú*, 112, 39-52.
916 DeVries, T.J., Jud, N.A. (2018). Lithofacies patterns and paleogeography of the Miocene Chilcatay
917 and lower Pisco depositional sequences (East Pisco Basin, Peru). *Boletín de la Sociedad*
918 *Geológica del Perú*, Volumen Jubilar 8, 124-167.
919 DeVries, T.J., Urbina, M., Jud, N.A. (2017). The Eocene-Oligocene Otuma depositional sequence
920 (East Pisco Basin, Peru): paleogeographic and paleoceanographic implications of new data.

Boletín de la Sociedad Geológica del Perú, 112, 14-38.

Di Celma, C., Malinverno, E., Bosio, G., Collareta, A., Gariboldi, K., Gioncada, A., Molli, G., Basso, D., Varas-Malca, R.M., Pierantoni, P.P., Villa I.M., Lambert, O., Landini, W., Sarti, G., Cantalamessa, G., Urbina, M., Bianucci, G. (2017). Sequence stratigraphy and paleontology of the upper Miocene Pisco Formation along the western side of the lower Ica valley (Ica Desert, Peru). *Rivista Italiana di Paleontologia e Stratigrafia*, 123, 255-274.

Di Celma, C., Malinverno, E., Cantalamessa, G., Gioncada, A., Bosio, G., Villa, I.M., Gariboldi, K., Rustichelli, A., Pierantoni, P.P., Landini, W., Tinelli, C., Collareta, A., Bianucci, G. (2016a). Stratigraphic framework of the late Miocene Pisco Formation at Cerro Los Quesos (Ica Desert, Peru). *Journal of Maps*, 12, 1020-1028.

Di Celma, C., Malinverno, E., Collareta, A., Bosio, G., Gariboldi, K., Lambert, O., Landini, W., Pierantoni, P.P., Gioncada, A., Villa, I.M., Coletti, G., Muizon, C. de, Urbina, M., Bianucci, G. (2018). Facies analysis, stratigraphy and marine vertebrate assemblage of the lower Miocene Chilcatay Formation at Ullujaya (Pisco basin, Peru). *Journal of Maps*, 14, 257-268.

Di Celma, C., Malinverno, E., Gariboldi, K., Gioncada, A., Rustichelli, A., Pierantoni, P.P., Landini,W., Bosio, G., Tinelli, C., Bianucci, G. (2016b). Stratigraphic framework of the late Miocene to Pliocene Pisco Formation at Cerro Colorado (Ica Desert, Peru). *Journal of Maps*, 12, 515-557.

Duffy, C., Gordon, I. (2003). *Carcharhinus brachyurus*. In: The IUCN Red List of Threatened Species 2003: e.T41741A10551730. http://www.iucnredlist.org, accessed on April 28, 2018.

Dunbar, R.B., Marty, R.C., Baker, P.A. (1990). Cenozoic marine sedimentation in the Sechura and Pisco basins, Peru. *Palaeogeography, Palaeoclimatology, Palaeoecology*, 77, 235-261.

Ehret, D.J., Macfadden, B.J., Jones, D.S., DeVries, T.J., Foster, D.A., Salas-Gismondi, R. (2012). Origin of the white shark *Carcharodon* (Lamniformes: Lamnidae) based on recalibration of the Upper Neogene Pisco Formation of Peru. *Palaeontology*, 55, 1139-1153.

946 Ehret, D.J., MacFadden, B.J., Salas-Gismondi, R. (2009). Caught in the act: trophic interactions
947 between a 4-million-year-old white shark (*Carcharodon*) and mysticete whale from Peru.
948 *Palaios*, 24, 329-333.
949 Eckert, K.L., Wallace, B.P., Frazier, J.G., Eckert, S.A., Pritchard, P.C.H. (2012). Synopsis of the
950 biological data on the leatherback sea turtle (*Dermochelys coriacea*). Jacksonville, U.S.
951 Department of Interior, Fish and Wildlife Service.
952 Esperante, R., Brand, L.R., Chadwick, A.V., Poma, O. (2015). Taphonomy and paleoenvironmental
953 conditions of deposition of fossil whales in the diatomaceous sediments of the Miocene/Pliocene
954 Pisco Formation, southern Peru—a new Fossil-Lagerstätte. *Palaeogeography,*
955 *Palaeoclimatology, Palaeoecology*, 417, 337-370.
956 Fallows, C., Gallagher, A.J., Hammerschlag, N. (2013). White sharks (*Carcharodon carcharias*)
957 scavenging on whales and its potential role in further shaping the ecology of an apex predator.
958 *PLOS ONE*, 8, article #e60797.
959 Fierstine, H.L. (2006). Fossil history of billfishes (Xiphioidei). *Bulletin of Marine Science*, 79, 433-
960 453.
961 Föllmi, K.B., Grimm, K.A. (1990). Doomed pioneers: Gravity-flow deposition and bioturbation in
962 marine dysaerobic environments. *Geology*, 18, 1069-1072.
963 Gariboldi, K., Gioncada, A., Bosio, G., Malinverno, E., Di Celma, C., Tinelli, C., Cantalamessa, G.,
964 Landini, W., Urbina, M., Bianucci, G. (2015). The dolomite nodules enclosing fossil marine
965 vertebrates in the East Pisco Basin, Peru: field and petrographic insights into the Lagerstätte
966 formation. *Palaeogeography, Palaeoclimatology, Palaeoecology*, 438, 81-95.
967 Gioncada, A., Collareta, A., Gariboldi, K., Lambert, O., Di Celma, C., Bonaccorsi, E., Urbina, M.,
968 Bianucci, G. (2016). Inside baleen: exceptional microstructure preservation in a late Miocene
969 whale skeleton from Peru. *Geology*, 44, 839-842.
970 Gioncada, A., Gariboldi, K., Collareta, A., Di Celma, C., Bosio, G., Malinverno, E., Lambert, O.,

971 Pike, J., Urbina, M., Bianucci, G. (2018). Looking for the key to preservation of fossil marine
972 vertebrates in the Pisco Formation of Peru: new insights from a small dolphin skeleton. *Andean*
973 *Geology*, 45, in press.
974 Gioncada, A., Petrini, R., Bosio, G., Gariboldi, K., Collareta, A., Malinverno, E., Bonaccorsi, E., Di
975 Celma, C., Pasero, M., Urbina, M., Bianucci, G. (2018). Insights into the diagenetic environment
976 of fossil marine vertebrates of the Pisco Formation (late Miocene, Peru) from mineralogical and
977 Sr-isotope data. *Journal of South American Earth Sciences*, 81, 141-152.
978 Hammer, Ø., Harper, D.A.T., Ryan, P. D. (2001). PAST: Paleontological statistics software package
979 for education and data analysis. *Palaeontologia Electronica*, 4.1.4:1-9.
980 Hampel, A., Kukowski, N., Bialas, J., Heubscher, C., Heinbockel, R. (2004). Ridge subduction at an
981 erosive margin: the collision zone of the Nazca Ridge in southern Peru. *Journal of Geophysical*
982 *Research*, 109. article #B02101.
983 Hernández-Molina, F.J., Fernández-Salas, L.M., Lobo, F., Somoza, L., Díaz-del-Río, V., Alverinho
984 Dias, J.M. (2000). The infralittoral prograding wedge: a new large-scale progradational
985 sedimentary body in shallow marine environments. *Geo-Marine Letters*, 20, 109-117.
986 James, N.P. (1997). The cool-water carbonate depositional realm. In: James, N.P., Clarke, J.A.D.
987 (Eds.), Cool-water Carbonates. *SEPM Special Publications*, 56, 1-20.
988 Jardas, I., Šantić, M., Armin, P. (2004). Diet composition of the eagle ray, *Myliobatis aquila*
989 (Chondrichthyes: Myliobatidae), in the eastern Adriatic. *Cybium*, 28, 372-374.
990 Kellogg, R. (1927). *Kentriodon pernix*, a Miocene porpoise from Maryland. *Proceedings of the*
991 *United States National Museum*, 69, 1-55.
992 Kellogg, R. (1932). A Miocene long-beaked porpoise from California. *Smithsonian Miscellaneous*
993 *Collections*, 87: 1-11.
994 Kidwell, S.M. (1991). Condensed deposits in siliciclastic sequences: Expected and observed
995 features. In: Einsele, G., Ricken,W., Seilacher, A. (Eds.), Cycles and events in stratigraphy.

996 Heidelberg, Springer-Verlag, 682-695.
997 Kidwell, S.M., Powars, D.S., Edwards, L.E., Vogt, P.R. (2015). Miocene stratigraphy and
998 paleoenvironments of the Calvert Cliffs, Maryland. *Geological Society of America Field Guide*,
999 40, 231-279.
1000 Kiel, S., Goedert, J.L., Kahl, W.-A., Rouse, G.W. (2010). Fossil traces of the bone-eating worm
1001 *Osedax* in early Oligocene whale bones. *PNAS*, 107, 8656-8659.
1002 Kitchell, J.F., Martell, S.J., Walters, C.J., Jensen, O.P., Kaplan, I.C., Watters, J., Essington, T.E.,
1003 Boggs, C.H. (2006). Billfishes in an ecosystem context. *Bulletin of Marine Science*, 79, 669-682.
1004 Kulm, L.D., Resig, J.M., Thornburg, T.M., Schrader, H.J. (1982). Cenozoic structure, stratigraphy
1005 and tectonics of the central Peru forearc. In: Legget J.K. (Ed.), Trench and forearc geology:
1006 sedimentation and tectonics on modern and ancient plate margins. London, Blackwells, 151-169.
1007 Lambert, O., Bianucci G., Muizon C de. (2017). Macroraptorial sperm whales (Cetacea, Odontoceti,
1008 Physeteroidea) from the Miocene of Peru. *Zoological Journal of the Linnean Society*, 179, 404-
1009 474.
1010 Lambert, O., Bianucci, G., Urbina, M. (2014). *Huaridelphis raimondii*, a new early Miocene
1011 Squalodelphinidae (Cetacea, odontoceti) from the Chilcatay Formation, Peru. *Journal of*
1012 *Vertebrate Paleontology*, 34, 987-1004.
1013 Lambert, O., Collareta, A., Landini, W., Post, K., Ramassamy, B., Di Celma, C., Urbina, M.,
1014 Bianucci, G. (2015a). No deep diving: evidence of predation on epipelagic fish for a stem beaked
1015 whale from the late Miocene of Peru. *Proceedings of the Royal Society of London B*, 202, article
1016 #20151530.
1017 Lambert, O., Gigase, P. (2007). A monodontid cetacean from the Early Pliocene of the North Sea.
1018 *Bulletin de l'Institut Royal des Sciences Naturelles de Belgique-Sciences de la Terre*, 77, 197-
1019 210.
1020 Lambert, O., Martínez-Cáceres, M., Bianucci, G., Di Celma, C., Salas-Gismondi, R., Steurbaut, E.,

1021 Urbina, M., Muizon, C. de (2017a). Earliest mysticete from the Late Eocene of Peru sheds new
1022 light on the origin of baleen whales. *Current Biology*, 27, 1535-1541.
1023 Lambert, O., Muizon, C. de, Bianucci, G. (2015b). A new archaic homodont toothed cetacean
1024 (Mammalia, Cetacea, Odontoceti) from the early Miocene of Peru. *Geodiversitas*, 37, 79-108.
1025 Lambert, O., Muizon, C. de, Malinverno, E., Celma, C. D., Urbina, M., Bianucci, G. (2018). A new
1026 odontocete (toothed cetacean) from the Early Miocene of Peru expands the morphological
1027 disparity of extinct heterodont dolphins. *Journal of Systematic Palaeontology*, 16(12), 981-1016.
1028 Landini, W., Altamirano-Sierra, A., Collareta, A., Di Celma, C., Urbina, M., Bianucci, G. (2017a).
1029 The new Late Miocene chondrichthyan assemblage from Cerro Colorado (Pisco Formation,
1030 Peru). *South American Journal of Earth Sciences*, 73, 168-190.
1031 Landini, W., Collareta, A., Pesci, F., Di Celma, C., Urbina, M., Bianucci, G. (2017b). A secondary
1032 nursery area for the copper shark *Carcharhinus brachyurus* from the late Miocene of Peru. *South*
1033 *American Journal of Earth Sciences*, 78, 164-174.
1034 Landini, W., Collareta, A., Di Celma, C., Malinverno, E., Urbina, M., Bianucci, G. (2018). The early
1035 Miocene elasmobranch assemblage from Zamaca (Chilcatay Formation, Peru). *South American*
1036 *Journal of Earth Sciences*, in press, DOI: 10.1016/j.jsames.2018.08.004.
1037 León, W., Aleman, A., Torres, V., Rosell, W., De la Cruz, O. (2008). Estratigrafía, sedimentología y
1038 evolución tectónica de la cuenca Pisco Oriental. *Boletín INGEMMET*, 27, 144 pp.
1039 Long, D.J., Jones, R.E. (1996). White shark predation and scavenging on cetaceans in the eastern
1040 North Pacific Ocean. In: Klimley, A.P., Ainley, D.G. (Eds.), Great white sharks: the biology of
1041 *Carcharodon carcharias*. San Diego, Academic Press, 293-307.
1042 Lucchi, F., Tranne, C.A., Rossi, P.L. (2010). Stratigraphic approach to geological mapping of the
1043 late Quaternary volcanic island of Lipari (Aeolian archipelago, southern Italy). *Geological*
1044 *Society of America Special Papers*, 464, 1-32.
1045 McCurry, M.R., Evans, A.R., Fitzgerald, E.M.G., Adams, J.W., Clausen, P.D., McHenry, C.R.

(2017). The remarkable convergence of skull shape in crocodilians and toothed whales. *Proceedings of the Royal Society of London B*, 284, article #20162348.

Manojkumar, P.P., Pavithran, P.P. (2004). First record of snaggletooth shark, *Hemipristis elongatus* (Klunzinger, 1871) from Malabar Coast. *Marine Fisheries Information Service, Technical and Extension Series*, 180, 13-14.

Marocco, R., Muizon, C. de, (1988). Le Bassin Pisco, bassin cénozoïque d'avant arc de la côte du Pérou central: analyse géodynamique de son remplissage. *Géodynamique*, 3, 3-19.

Marx, F.G., Fordyce, R.E. (2015). Baleen boom and bust: a synthesis of mysticete phylogeny, diversity and disparity. *Royal Society Open Science*, 2, article #140434.

Marx, F.G., Uhen, M.D. (2010). Climate, critters, and cetaceans: Cenozoic drivers of the evolution of modern whales. *Science*, 327, 993-996.

Martínez-Cáceres, M., Lambert, O., Muizon, C. de (2017). The anatomy and phylogenetic affinities of *Cynthiacetus peruvianus*, a large *Dorudon*-like basilosaurid (Cetacea, Mammalia) from the late Eocene of Peru. *Geodiversitas*, 39, 7-163.

Massari, F., Chiocci, F. (2006). Biocalcarenite and mixed cool-water prograding bodies of the Mediterranean Pliocene and Pleistocene: architecture, depositional setting and forcing factors. In: Pedley, H.M., Carannante, G. (Eds.), Cool-water carbonates: depositional systems and palaeoenvironmental controls. *Geological Society, London, Special Publications*, 255, 95-120.

Massari, F., D'Alessandro, A. (2012) Facies partitioning and sequence stratigraphy of a mixed siliciclastic-carbonate ramp stack in the Gelasian of Sicily (S Italy): a potential model for icehouse, distally steepened heterozoan ramps. *Rivista Italiana di Paleontologia e Stratigrafia*, 118, 503-534.

Mitchell, N.C., Masselink, G., Huthnance, J.M., Fernández-Salas, L.M., Lobo, F.J. (2012) Depths of modern coastal sand clinoforms. *Journal of Sedimentary Research*, 82, 469-481.

Molina, J.M., Cazorla, A.L. (2015). Biology of *Myliobatis goodei* (Springer, 1939), a widely

distributed eagle ray, caught in northern Patagonia. *Journal of Sea Research*, 95, 106-114.

Noriega, J.I., Cione, A.L., Aceñolaza, F.G. (2007). Shark tooth marks on Miocene balaenopterid cetacean bones from Argentina. *Neues Jahrbuch für Geologie und Paläontologie-Abhandlungen*, 245, 185-192.

Norris, R.D, Kirtland Turner, S., Hull, P.M, Ridgwell, A. (2013). Marine ecosystem responses to Cenozoic global change. *Science*, 341, 492–498.

Peverell, S.C. (2009). Sawfish (Pristidae) of the Gulf of Carpentaria, Queensland, Australia. Unpublished MSc thesis, James Cook University (Australia), 147 pp.

Pickering, K.T., Hiscott, R.N., Hein, F.J. (1989). Deep-marine environments: clastic sedimentation and tectonics. London, Unwin Hyman.

Pimiento, C., MacFadden, B.J., Clements, C.F., Varela, S., Jaramillo, C., Velez-Juarbe, J., Silliman, B.R. (2016). Geographical distribution patterns of *Carcharocles megalodon* over time reveal clues about extinction mechanisms. *Journal of Biogeography*, 43, 1645-1655.

Pomar, L., Aurell, M., Bádenas, B., Morsilli, M., Al-Awwad, S.F. (2015) Depositional model for a prograding oolitic wedge, Upper Jurassic, Iberian basin. *Marine and Petroleum Geology*, 67, 556-582.

Pomar, L., Kendall, C. G. St. C. (2008). Carbonate platform architecture; a response to hydrodynamics and evolving ecology. In: Lukasik, J., Simo, T. (Eds.), Controls on carbonate platform and reef development. *SEPM Special Publication*, 89, 187-216.

Pomar, L., Tropeano, M. (2001) The calcarenite di Gravina Formation in Matera (southern Italy): new insights for coarse-grained, large scale, cross-bedded bodies encased in offshore deposits. *AAPG Bulletin*, 85, 661-689.

Pratt, H.L., Jr., Casey, J.G., Conklin, R.B. (1982). Observations on large white shark, *Carcharodon carcharias*, off Long Island, New York. *Fishery Bulletin*, 80, 153-156.

Purdy, R.W., Schneider, V.P., Applegate, S.P., Mclellan, J.H., Meyer, R.L., Slaughter, R. 2001.The

1096 Neogene sharks, rays, and bony fishes from Lee Creek Mine, Aurora, North Carolina. In: Ray,
1097 C.E., Bohaska, D.J. (Eds.), Geology and paleontology of the Lee Creek Mine, North Carolina,
1098 III. *Smithsonian Contributions to Paleobiology*, 90, 71-202.
1099 Pyenson, N.D., Irmis, R.B., Lipps, J.H., Barnes, L.G., Mitchell Jr, E.D., McLeod, S.A. (2009).
1100 Origin of a widespread marine bonebed deposited during the middle Miocene Climatic
1101 Optimum. *Geology*, 37, 519-522.
1102 Raiswell, R., Berner, R.A. (1985). Pyrite formation in euxinic and semi-euxinic sediments.
1103 *American Journal of Science*, 285, 710-724.
1104 Ramassamy, B., Lambert, O., Collareta, A., Urbina, M., Bianucci, G. (2018). Description of the
1105 skeleton of the fossil beaked whale *Messapicetus gregarius*, searching potential proxies for deep
1106 diving abilities. *Fossil Record*, 21, 11-32.
1107 Reisdorf, A.G., Anderson, G.S., Bell, L.S., Klug, C., Schmid-Röhl, A., Röhl, H.J., Jung, M., Wuttke,
1108 M., Maisch, M.W., Benecke, M., Wyler, D., Bux, R., Fornaro, P., Wetzel, A. 2014. Reply to
1109 "Ichthyosaur embryos outside the mother body: not due to carcass explosion but to carcass
1110 implosion" by van Loon (2013). *Palaeobiodiversity and Palaeoenvironments*, 94, 487-494.
1111 Rezende, G.A. de, Capitoli, R.R., Vooren, C.M. (2015). Dieta e morfologia da cabeça, boca e
1112 dentição de duas raias simpátricas, *Myliobatis goodei* e *M. ridens* (Batoidea: Myliobatiformes).
1113 *Boletim do Museu de Biologia Mello Leitão*, 37, 255-270.
1114 Rivera, T.A., Storey, M., Zeeden, C., Hilgen, F.J., Kuiper, K. (2011). A refined astronomically
1115 calibrated $^{40}Ar/^{39}Ar$ age for Fish Canyon sanidine. *Earth and Planetary Science Letters*, 311,
1116 420-426.
1117 Rustichelli, A., Di Celma, C., Tondi, E., Baud, P., Vinciguerra, S. (2016a). Fibrous gypsum veins as
1118 diffuse features and within fault zones: the case study of the Pisco Basin (Ica desert, southern
1119 Peru). *Journal of the Geological Society*, 173, 405-418.
1120 Rustichelli, A., Di Celma, C., Tondi, E., Bianucci, G. (2016b). Deformation within the Pisco basin

1121 sedimentary record (southern Peru): Stratabound orthogonal vein sets and their impact on fault
1122 development. *Journal of South American Earth Sciences*, 65, 79-100.
1123 Santini, F., Carnevale, G., Sorenson, L. (2013). First molecular scombrid timetree (Percomorpha:
1124 Scombridae) shows recent radiation of tunas following invasion of pelagic habitat. *Italian*
1125 *Journal of Zoology*, 80, 210-221.
1126 Schäfer, W. (1972). Ecology and palaeoecology of marine environments. Chicago, University of
1127 Chicago Press.
1128 Shimada, K., Chandler, R.E., Lam, O.L.T., Tanaka, T., Ward, D.J. (2017). A new elusive otodontid
1129 shark (Lamniformes: Otodontidae) from the lower Miocene, and comments on the taxonomy of
1130 otodontid genera, including the 'megatoothed'clade. *Historical Biology*, 29, 704-714.
1131 Simpfendorfer, C.A., Burgess, G.H. (2009). *Carcharhinus leucas*. In: The IUCN Red List of
1132 Threatened Species 2013: e.T39372A10187195. http://www.iucnredlist.org, accessed on April
1133 28, 2018.
1134 Smile, M.J. (1991). Occurrence and feeding of three shark species, *Carcharhinus brachiurus*, *C.*
1135 *obscurus* and *Sphyrna zygaena*, on the Eastern Cape coast of South Africa. *South African*
1136 *Journal of Marine Science*, 11, 31-42.
1137 Smith, C.R., Glover, A.G., Treude, T., Higgs, N.D., Amon, D.J. (2015). Whale-fall ecosystems:
1138 recent insights into ecology, paleoecology, and evolution. *Annual Review of Marine Science*, 7,
1139 571-596.
1140 Thornburg, T.M., Kulm, L.D. (1981). Sedimentary basins of the Peru continental margin: structure,
1141 stratigraphy, and Cenozoic tectonics from 6ºS to 16ºS latitude. In: Kulm, L.D., Dymond, J.,
1142 Dasch, E.J., Hussong, D.M. (Eds.), Nazca plate: crustal formation and Andean convergence.
1143 *Geological Society of America Memoir*, 154, 393-422.
1144 Travis, R.B., Gonzales, G., Pardo, A. (1976). Hydrocarbon potential of coastal basins of Peru. In:
1145 Halbouty, M., Maher, J., Lian, H.M. (Eds.), Circum-Pacific energy and mineral resources. *AAPG*

1146 *Memoir*, 25, 331-338.
1147 Uhen, M.D., Pyenson, N.D., DeVries, T.J., Urbina, M., Renne, P.R. (2011). New middle Eocene
1148 whales from the Pisco Basin of Peru. *Journal of Paleontology*, 85, 955-969.
1149 Villa, I.M., Hermann, J., Müntener, O., Trommsdorff, V. (2000). $^{39}Ar/^{40}Ar$ dating of multiply zoned
1150 amphibole generations (Malenco, Italian Alps). *Contributions to Mineralogy and Petrology*, 140,
1151 363-381.
1152 Villa, I.M., Ruggieri, G., Puxeddu, M., Bertini, G. (2006). Geochronology and isotope transport
1153 systematics in a subsurface granite from the Larderello-Travale geothermal system (Italy).
1154 *Journal of Volcanology and Geothermal Research*, 152, 20-50.
1155 Viveen, W., Schlunegger, F. (2018) Prolonged extension and subsidence of the Peruvian forearc
1156 during the Cenozoic. *Tectonophysics*, 730, 48-62.
1157 von Huene, R., Lallemand, S. (1990). Tectonic erosion along the Japan and Peru convergent
1158 margins. *Geological Society of America Bulletin*, 102, 704-720.
1159 Whitmore Jr, F.C., Kaltenbach, J.A. (2008). Neogene Cetacea of the Lee Creek Phosphate Mine,
1160 North Carolina. *Virginia Museum of Natural History Special Publication*, 14, 181-269.
1161 Wilkin, R. T., Barnes, H. L., Brantley, S. L. (1996). The size distribution of framboidal pyrite in
1162 modern sediments: an indicator of redox conditions. *Geochimica et Cosmochimica Acta*, 60,
1163 3897-3912.
1164 Wood, R. C., Johnson-Gove, J., Gaffney, E. S., Maley, K. F. (1996). Evolution and phylogeny of the
1165 leatherback turtles (Dermochelyidae), with descriptions of new fossil taxa. *Chelonian*
1166 *Conservation and Biology*, 2, 266-286.
1167 Wueringer, B.E., Squire, L., Collin, S.P. (2009). The biology of extinct and extant sawfish
1168 (Batoidea: Sclerorhynchidae and Pristidae). *Reviews in Fish Biology and Fisheries*, 19, 445-464.
1169 Zúñiga-Rivero, F.J., Klein, G.D., Hay-Roe, H., Álvarez-Calderon, E. (2010). The hydrocarbon
1170 potential of Peru. Lima, BPZ Exploración & Producción S.R.L.

Table captions

Table 1. Overview of the lower Miocene marine vertebrate assemblage from *Ct1a* of the Chilcatay Formation exposed at Ullujaya, with a summary of the main taphonomic features of the fossil specimens. Isolated teeth and spines of Elasmobranchii and scales of Osteichthyes are not considered. Field numbers are after Di Celma et al. (2018). Abbreviation: Height abs = Height above the base of the section. Precise geographic coordinates of individual specimens are available on request from the corresponding author.

Table 2. Composition of the lower Miocene elasmobranch assemblage from *Ct1a* of the Chilcatay Formation exposed at Ullujaya.

Table 3. General prospect of the vertebrate specimens selected for the microscopic analyses, with a summary of the macro- and microscopic taphonomic features of the bones.

Table 4. Synoptic comparison of the main diversified lower Miocene cetacean assemblages worldwide. See main text for data sources.

Figure captions

Figure 1. A) Sketch map of the major sedimentary basins of coastal Peru showing the position of both the Outer Shelf Ridge and Upper Slope Ridge, redrawn and modified from Travis et al. (1976) and Thornburg & Kulm (1981). The red dashed rectangle outlines the location of the area shown in detail in Fig. 1B. B) Inferred palaeogeographic map of the EPB during the Miocene (redrawn and modified from Marocco and Muizon, 1988). This basin was a semi-enclosed, shallow littoral embayment partially separated from the open ocean by a chain of basement islands (the Gran Tablazo Archipelago of DeVries & Jud, 2018) of the emerging Outer Shelf Ridge. C) Close-up of the red dashed inset box in Fig. 1B showing the geographic location of the study area along the western side of the lower Ica valley.

Figure 2. A) Schematic stratigraphic column exhibiting the formational lithostratigraphy and the main component units of the Miocene portion of the basin fill of the EPB (not to scale). B) Simplified geological map showing the whole fossil vertebrate distribution for part of the Miocene succession exposed at Ullujaya (modified after Di Celma et al., 2018). C) Close- up of the black solid inset box in Fig. 2B further detailing the distribution of several tens of fossil vertebrate specimens at Ullujaya. D) Measured stratigraphic section. Note that, in the study area, all the allostratigraphic units dip gently towards NE. Clinoforms of *Ct1b* dip towards SW.

Figure 3. Field photographs. A) Depositional-dip oriented annotated panoramic view of the upper part of the Chilcatay Formation and the overlying Pisco Formation near Cerro Las Tres Piramides (geographic coordinates: 14°35'22"S, 75°38'20"W). The principal surfaces used to further subdivide the Chilcatay Formation into allomembers and the internal facies architecture

are indicated. Clinoforms of *Ct1b* prograde basinwards, showing truncated tops and typical downlapping basal contact onto subhorizontal and finer grained sediments of *Ct1a*. The Ct2 allomember rests on the CE0.2 unconformity and exhibits a pronounced retrogradational (fining-upward) facies trend. The Chilcatay and Pisco formations are separated by the PE0.0 unconformity. B) A 8-m-thick interval of siltstones and sandy siltstones that typify *Ct1a*. Note, just above the 1.8 m-long logging pole (encircled), the occurrence of a dark, granule-size conglomerate (black arrows) demarcated at its base by a conspicuous assemblage of moderate- to large-diameter *Thalassinoides* and *Gyrolithes* burrows (white arrows). These coarse grained beds indicate rare high-energy events that swept fragmented shells and small clasts into an otherwise quiescent environment. C-D) Close-up views of beds of shell debris and granule-size conglomerate intercalated within*Ct1a*. Note as subjacent silty strata are cut by a dense network of *Thalassinoides* and *Gyrolithes* burrows (white arrows) forming a *Glossifungites* suite. Burrows emanate from the base of the shell debris and granule-size conglomerate beds (dashed white line) and are infilled with overlying sediment.

Figure 4. Optical photos (A, B) and backscattered Scanning Electron Microscope (C, D) images of pyrite relics from the sediments of *Ct1a*. A) Rhombohedral crystals of dolomite associated with relics of pyrite framboids. B) Spherical relics of pyrite framboids. C) Rhombohedral crystals of dolomite. D) Detail of the framboidal texture of a pyrite relic.

Figure 5. Histograms of the size distribution of framboids in *Ct1a*, between 22 and 28.5 m abs. The number of pyrite framboids relics (N), the mean of framboid diameter, the Standard Deviation (SD) of the mean, and the percentage of framboids with a diameter greater than 10 μm are shown for each sample. Note the different distribution in the UL-D3 histogram with respect to the other samples.

Figure 6. A) Stratigraphic distribution of fossil vertebrates from *Ct1a* of the Chilcatay Formation exposed at Ullujaya. B) Quantitative composition of the fossil vertebrate assemblage of *Ct1a*, based on systematic surface prospecting (teeth and spines of Elasmobranchii are not considered). C) Quantitative composition of the fossil shark and ray assemblage from the *Ct1a* facies association, based on more than one thousand isolated teeth and spines.

Figure 7. Elasmobranch remains from *Ct1a* of the Chilcatay Formation exposed at Ullujaya. A) *Carcharocles chubutensis*. B) *Megalolamna paradoxodon*. C-D) *Cosmopolitodus hastalis*. E-F) I*surus oxyrinchus*. G) *Anotodus agassizii*. H) *Hemipristis serra*. I) *Alopias superciliosus*. J) *Physogaleus contortus*. K) *Galeocerdo aduncus*. L) *Carcharhinus* cf. *leucas*. M-N) *Carcharhinus brachyurus*. O-P) cf. *Myliobatis* sp. A-N) Lingual view. O) Occlusal view. P) Basal view.

Figure 8. Bedding view of fossil cetaceans from *Ct1a* of the Chilcatay Formation exposed at Ullujaya. A) Isolated cranium of *Kentriodon* sp. disposed ventral side-up position (field number: O7). B) Four associated and disarticulated vertebrae of aff. Odontoceti indet. (O57) and C) corresponding explanatory line drawing. D) Few associated and disarticulated bones (including mandibles and some vertebrae and ribs) of Odontoceti indet. (O29) and E) corresponding explanatory line drawing. F) Partial skeleton (including articulated vertebrae and disarticulated ribs and other fragmentary bones) of aff. Odontoceti indet. (O59) and G) corresponding explanatory line drawing. H) Fully disarticulated partial skeleton (including mandibles, humerus, ulna, vertebrae, and ribs.) of Squalodelphinidae indet. (O4) and G) corresponding explanatory line drawing. J) Seven articulated vertebrae of aff. Odontoceti indet. (O38) and K) Corresponding explanatory line drawing.

Figure 9. Fossil cetaceans (A-B, F-I) and tuna-like bony fish (C-E) from *Ct1a* of the Chilcatay Formation exposed at Ullujaya. Specimens depicted in panels F-I are exposed on vertical sections and exhibit evidence of partial sinking into the substratum. A) Disarticulated cranium, mandibles, and two ribs of an undescribed specimen of *Chilcacetus cavirhinus* (field number: O5; catalogue number: MUSM 2527) and B) corresponding explanatory line drawing. C) Fully articulated caudal fin (T2). D) Some associated and partially disarticulated vertebrae (T5). E) Few associated and partially disarticulated vertebrae and rays (T6). F) Three associated and disarticulated vertebrae of aff. Odontoceti indet. (field number: O40) with sunk transverse processes and G) corresponding explanatory line drawing. H) Partially articulated vertebral column of aff. Odontoceti indet. (O50) that moderately sank and I) corresponding explanatory line drawing. Red arrows indicate sinking of some portions of the bones.

Figure 10. Bubble plot of articulation versus completeness for the marine vertebrate assemblage from *Ct1a* of the Chilcatay Formation exposed at Ullujaya. Abbreviations: r^2 = Pearson's r-squared value; rs = Spearman rank-order correlation coefficient; T = intersect of the best-fit linear trend line with the completeness axis. For more details see chapter 3 of the present work and Beardmore et al. (2012).

Figure 11. Optical photos (A, B) and backscattered Scanning Electron Microscope images (C, F) of fossil marine mammal bones from *Ct1a* of the Chilcatay Formation exposed at Ullujaya. A) Detail of calcite cementing both the cancellous and the compact bone cavities of specimen O5; note that calcite started to grow from the surface of the bone trabecolae. B) Microborings on the bone surface of specimen O3. C) Transverse thin section in transmitted light of a rib from specimen O3; both cancellous and compact bone are visible. D) Reddish color of the bone surface of specimen O52 caused by the presence of Fe-oxyhydroxides. E) Cancellous bone of a

rib of specimen O5 showing an infill of sediment in some marrow cavities cemented by calcite. F) Microborings of the B-type (*sensu* Gariboldi et al., 2015) on the surface of a rib of specimen O3.

Figure 12. Evidences of fracturing on fossil cetaceans from *Ct1a* of the Chilcatay Formation exposed at Ullujaya. A) Cranium of *Kentriodon* sp. (MUSM 631) in lateral view, exhibiting a damaged posterior portion. B) The same in posterior view. C) Cranium of the holotype of of *Huaridelphis raimondii* (MUSM 1396) in lateral view, exhibiting weak fractures of the occipital shield and temporal region. D) The same in posterior view. Yellow arrows indicate the main direction of compression that originated the observed fracturing patterns.

Figure 13. Fossil cetacean bones displaying shark bite marks from *Ct1a* of the Chilcatay Formation exposed at Ullujaya. A-C and E-G) *Chilcacetus cavirhinus* (MUSM 2527). H-L). *Chilcacetus cavirhinus* (MUSM 1401). M-N) *Huaridelphis raimondii* (MUSM 1403). O) *Kentriodon* sp. A) Rib. B) Left humerus in medial view. C) The same in lateral view. D) Dried jaws of extant *Isurus oxyrinchus*. E) Sketch showing the shark gasping the flipper of the dolphin. F, G) Sketch showing the possible attack sequence, with the shark that bites the abdomen of the dolphin (F) before biting its flipper (G). H) Incomplete mandible in lateral view. I-N) Fragmentary ribs. O) Cranium in dorsal view.

Figure 14. Stylised reconstruction of the early Miocene marine vertebrate fauna of Ullujaya during deposition of *Ct1a*, highlighting the diversity of the assemblage described in the present work. Different species are shown as silhouettes, and are roughly to scale. Sediments belonging to *Ct1a* and *Ct1b* are cream and brown, respectively.

Figure 15. Diagram of framboid size distribution as a result of euxinic or oxic-dysoxic conditions. Data on modern euxinic and oxic-dysoxic environments are from Wilkin et al. (1996). Following the example of Agbi et al. (2015), these literature data are compared with our results. Samples from *Ct1a* provide evidence of the alternation of euxinic and oxic-dysoxic conditions at the seafloor.

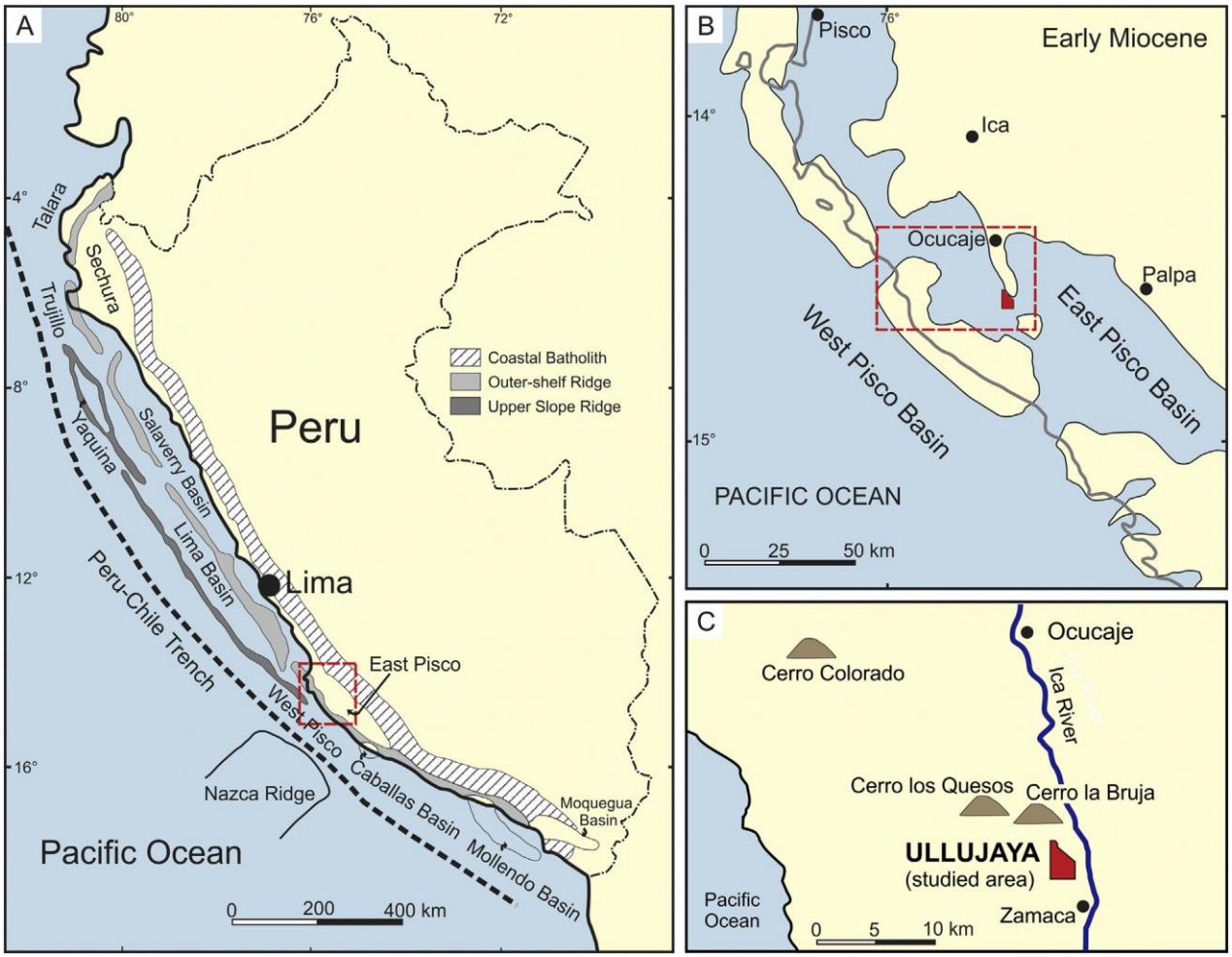
A
80°
76°
72°
4°
8°
12°
16°
Talara
Sechura
Trujillo
Yaquina
Salaverry Basin
Lima Basin
Peru-Chile Trench
Peru
Coastal Batholith
Outer-shelf Ridge
Upper Slope Ridge
Lima
East Pisco
West Pisco
Caballas Basin
Nazca Ridge
Moquegua Basin
Mollendo Basin
Pacific Ocean
0 200 400 km
B
Pisco
76°
Early Miocene
14°
Ica
Ocucaje
Palpa
East Pisco Basin
West Pisco Basin
15°
PACIFIC OCEAN
0 25 50 km
C
Ocucaje
Cerro Colorado
Ica River
Cerro los Quesos
Cerro la Bruja
ULLUJAYA
(studied area)
Pacific Ocean
Zamaca
0 5 10 km

Figure 1

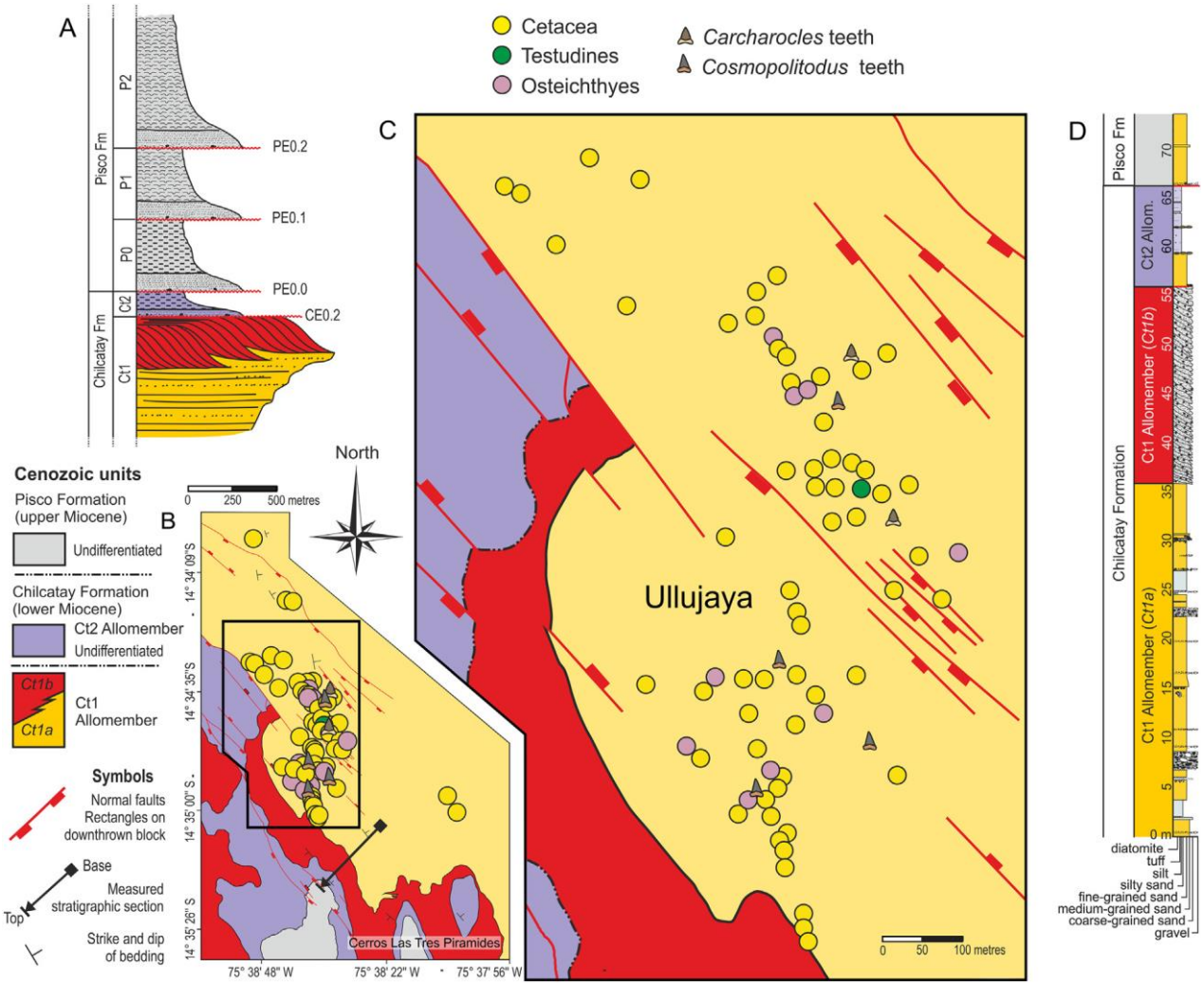

1323

1324

1325 Figure 2

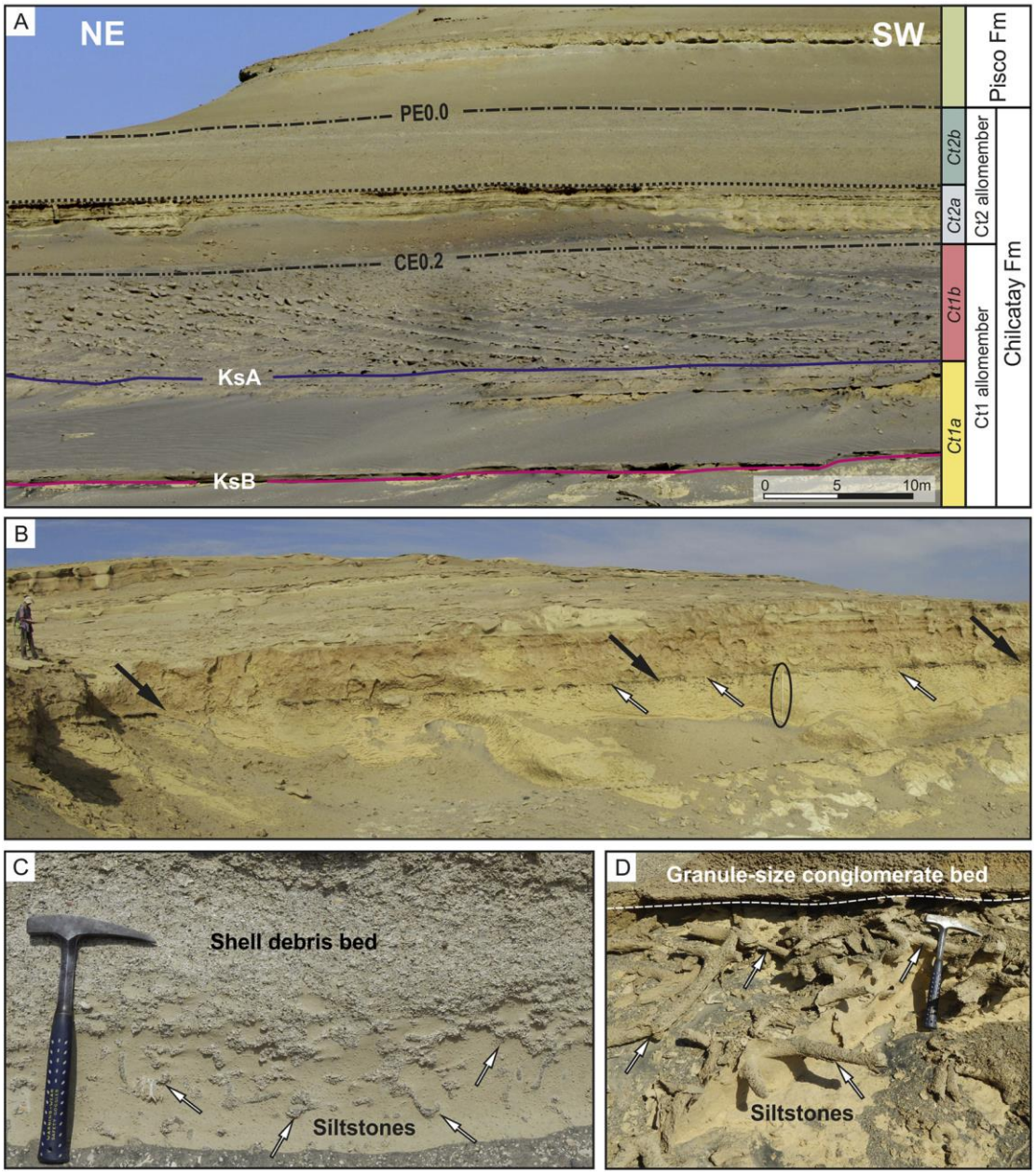

1326

1327 Figure 3

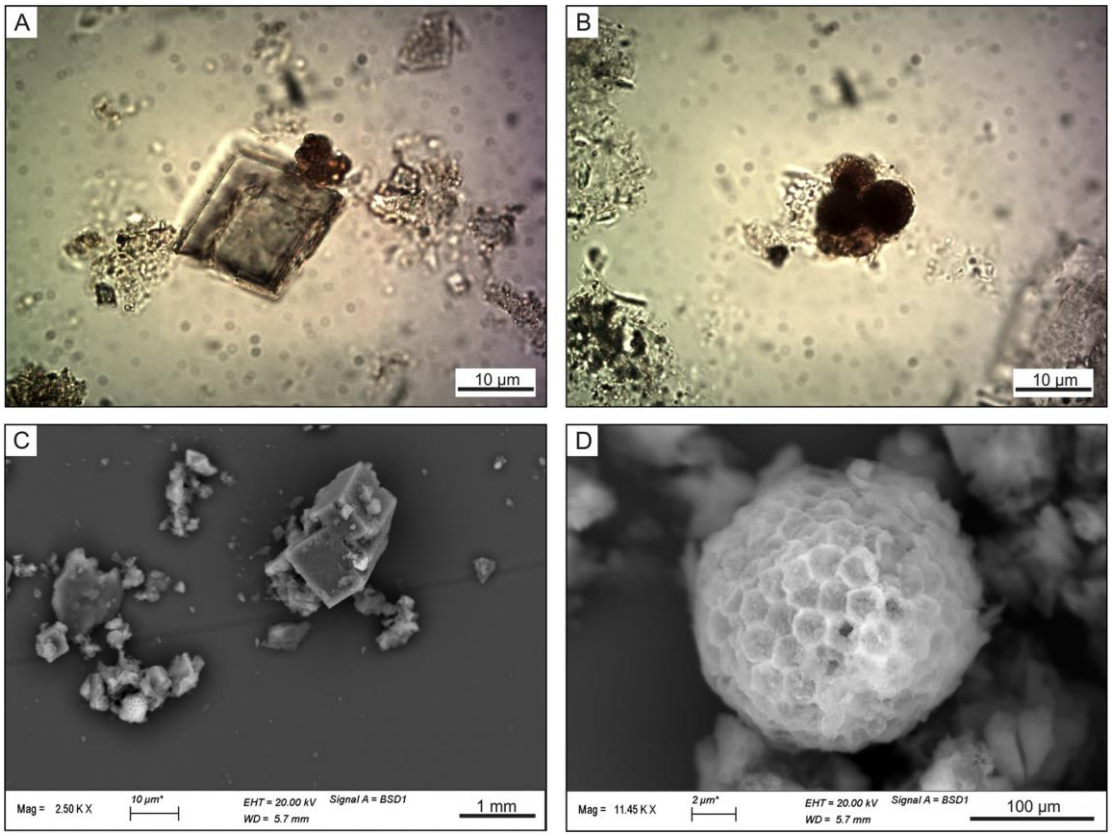

1328

1329 Figure 4

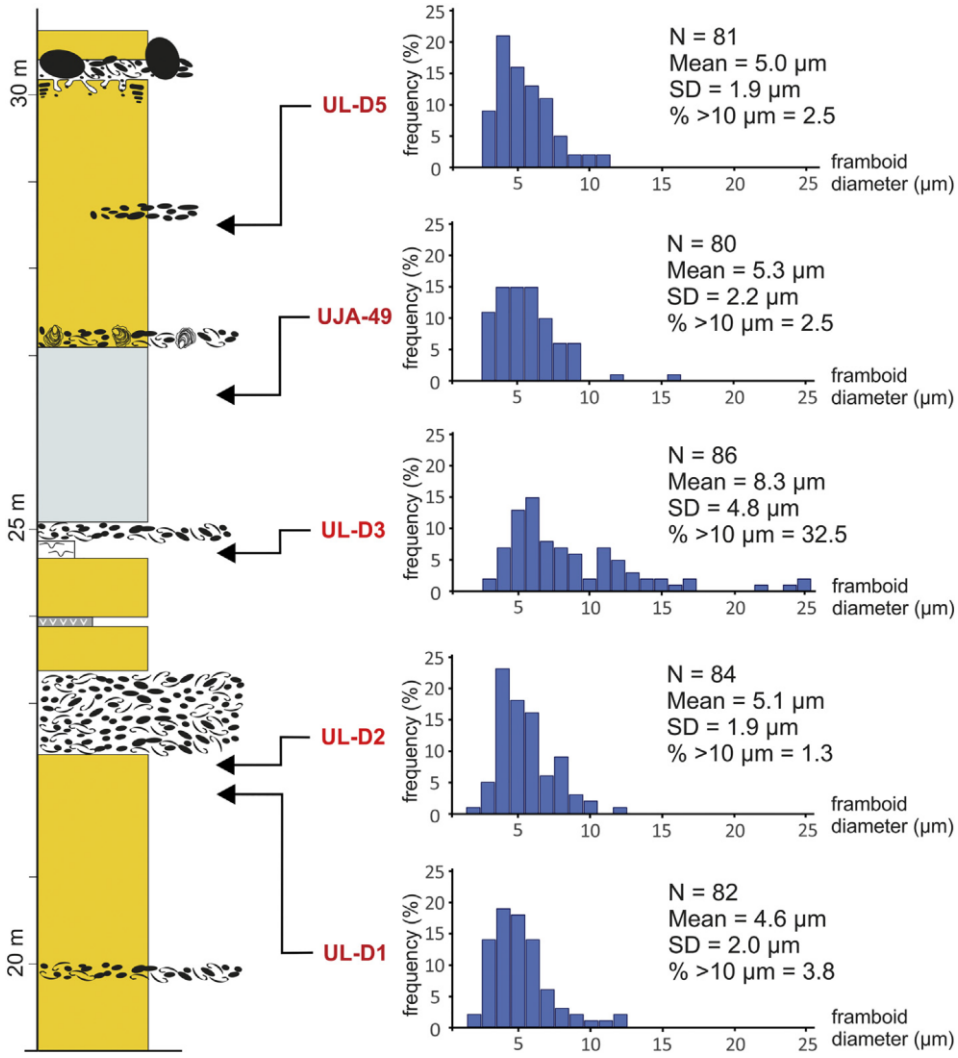

1330

1331 Figure 5

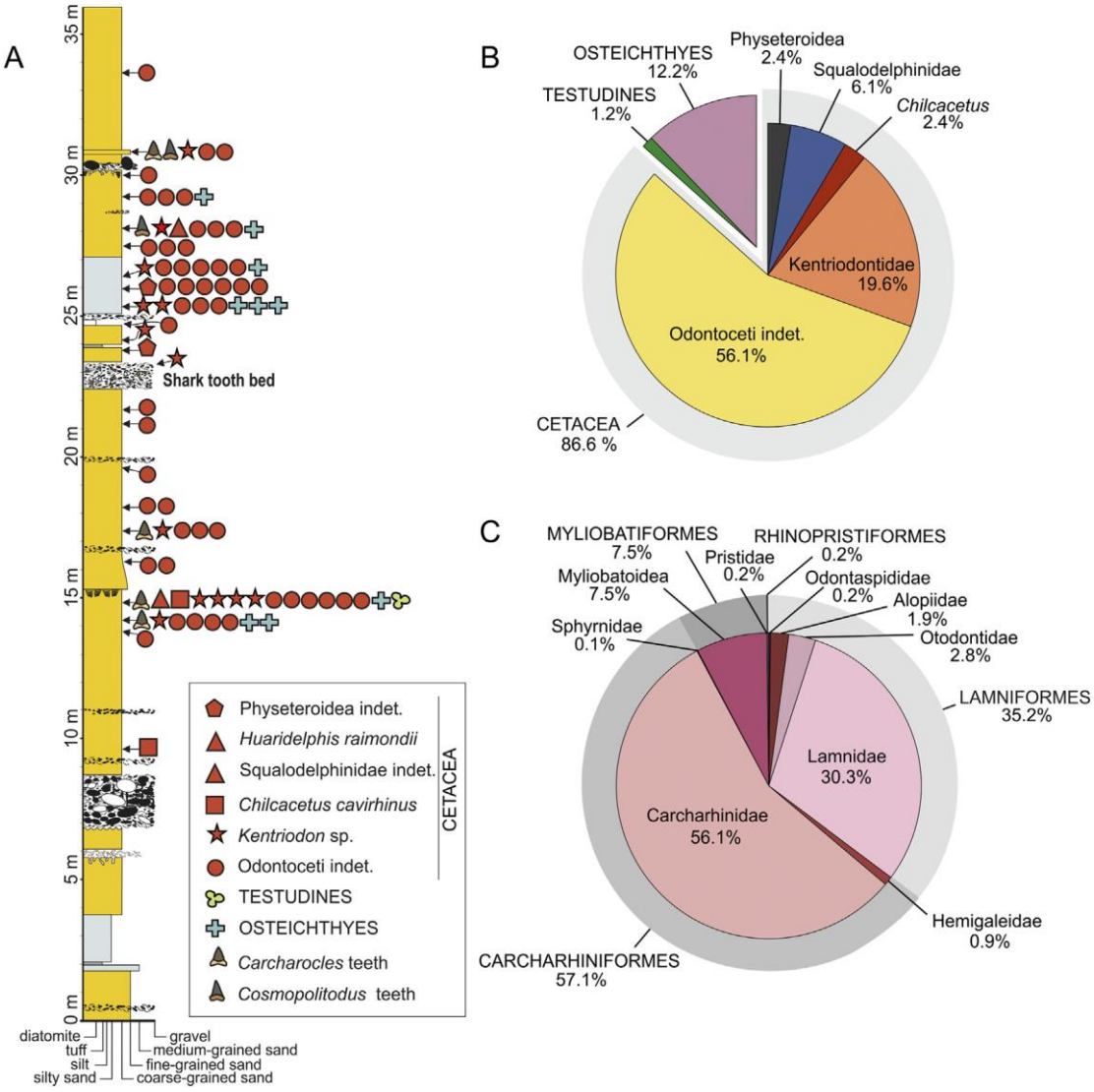

1332

1333 Figure 6

1334

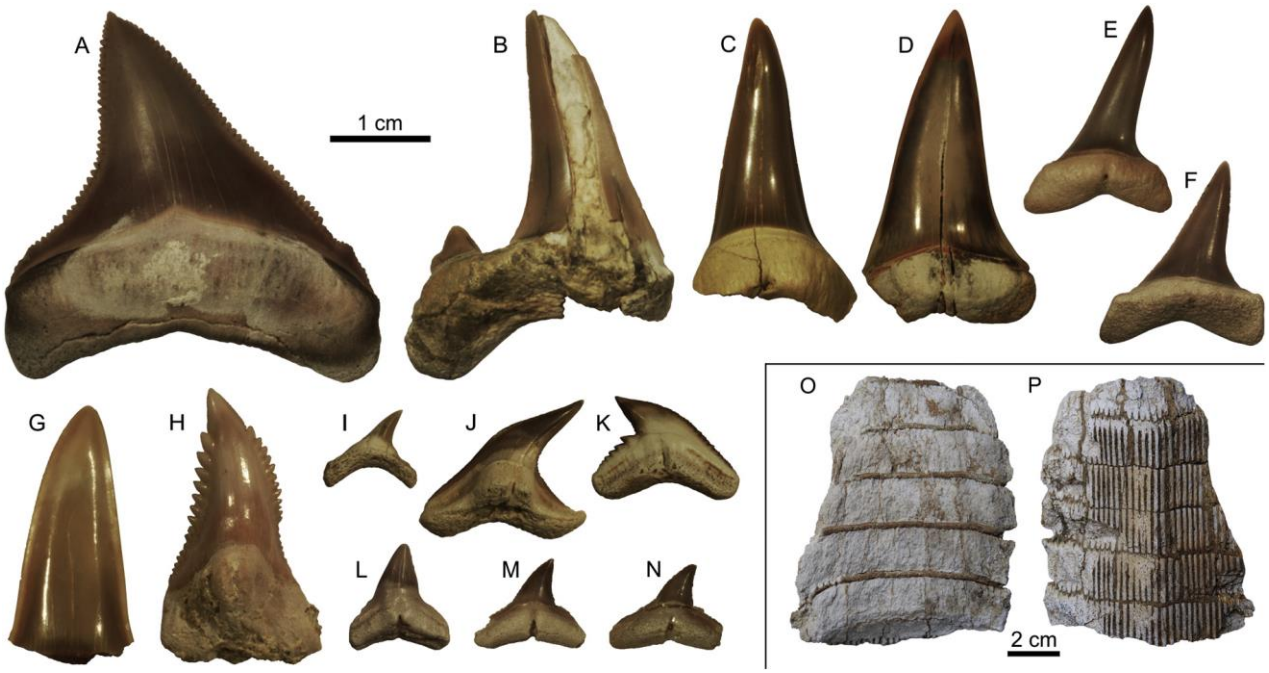

Figure 7

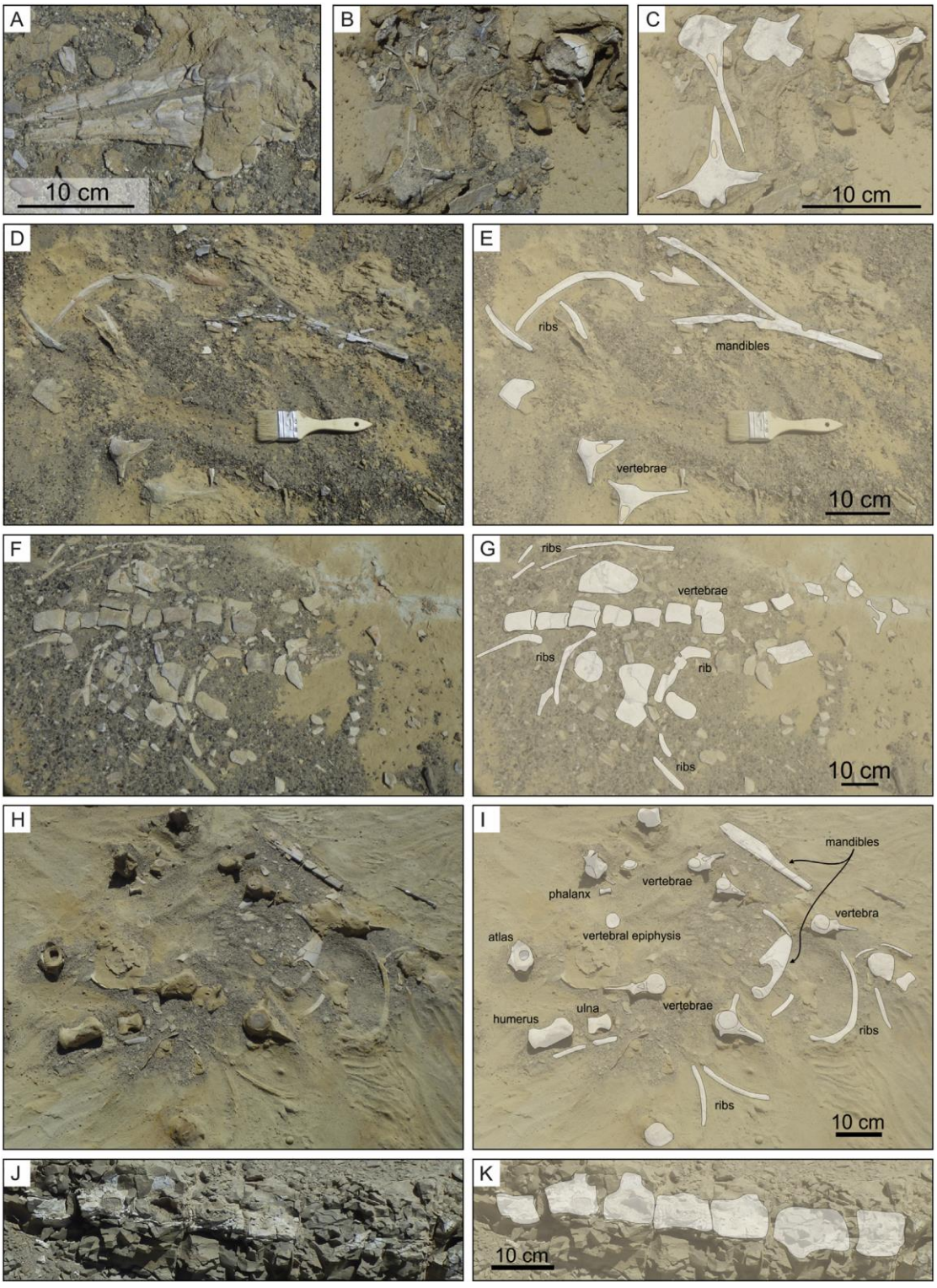

1337

1338 Figure 8

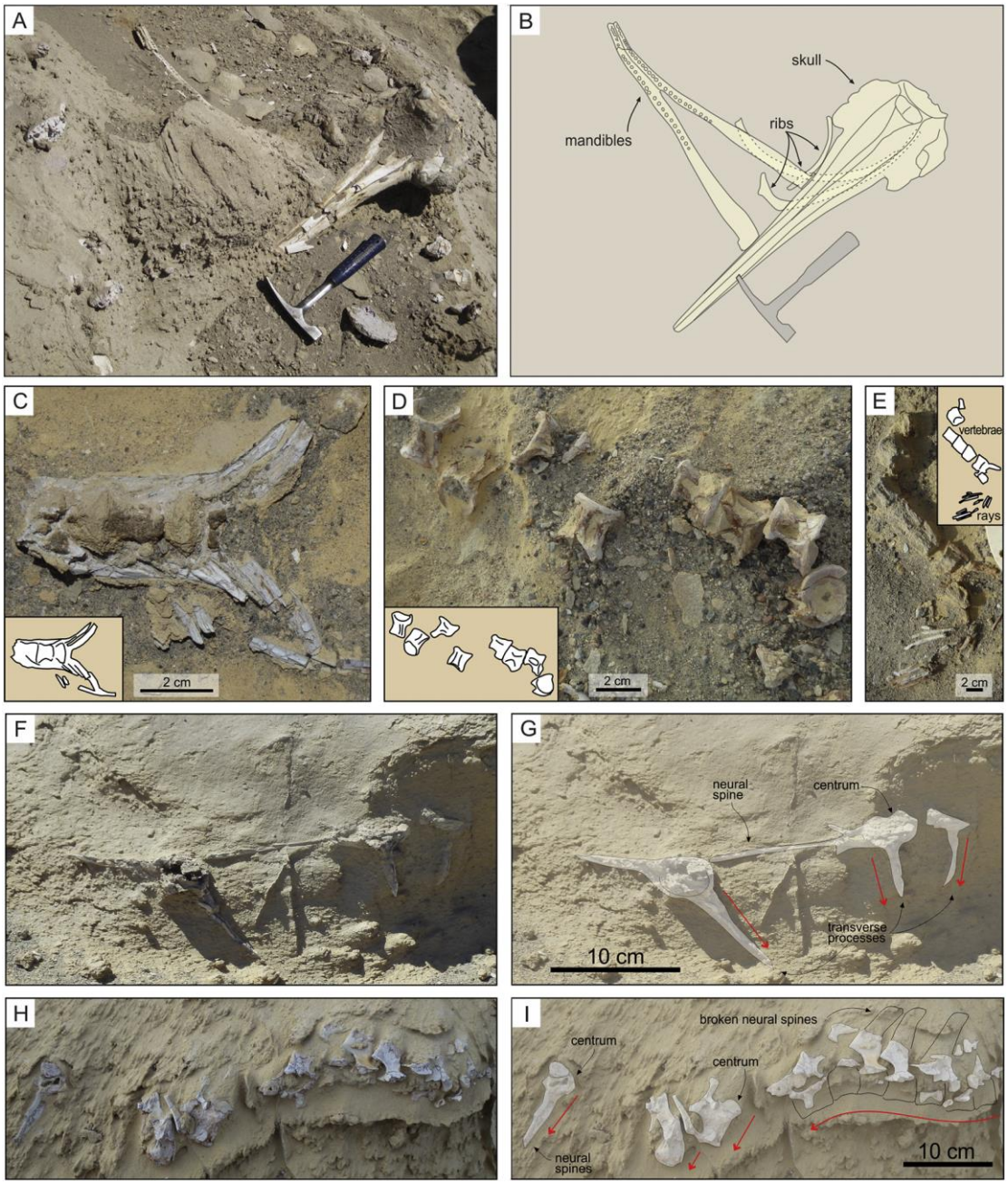

1339

1340 Figure 9

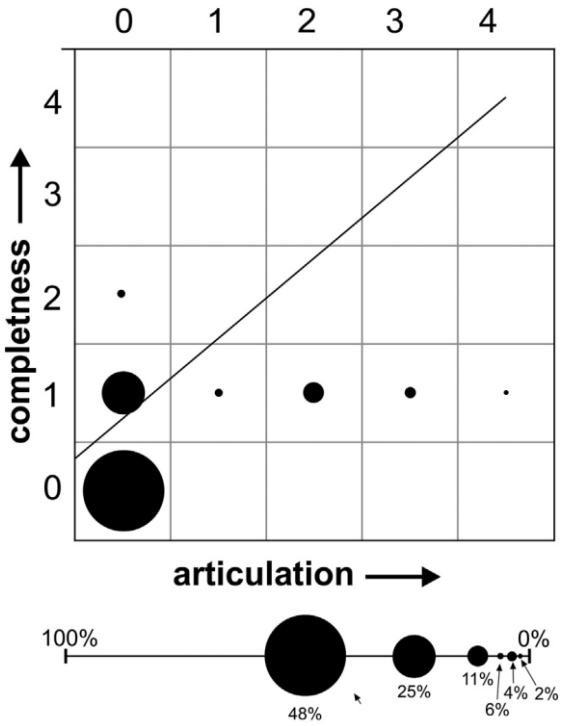

1341 r^2 = 1.38, rs = 0.47, T = 0.30

1342 Figure 10

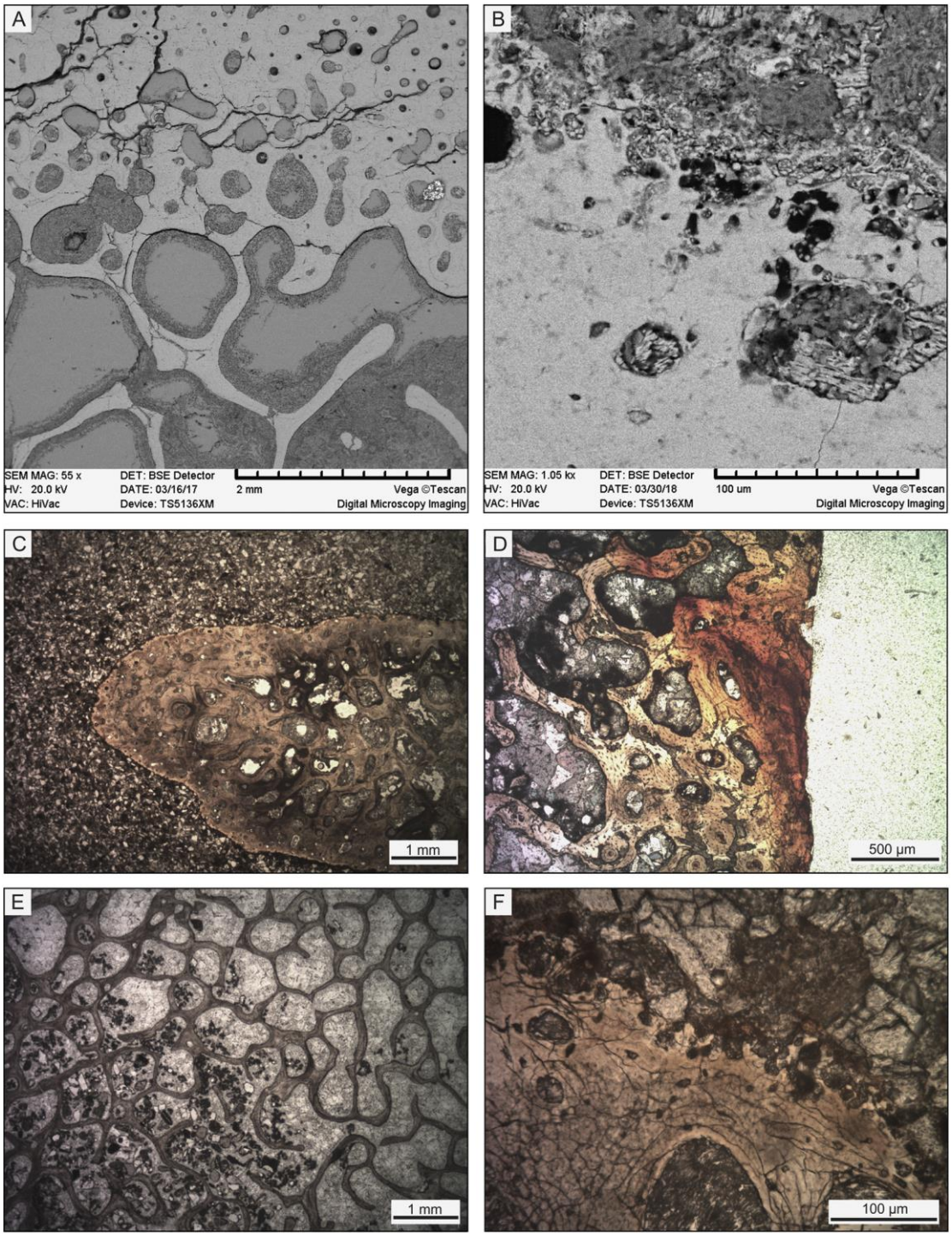

1343

1344 Figure 11

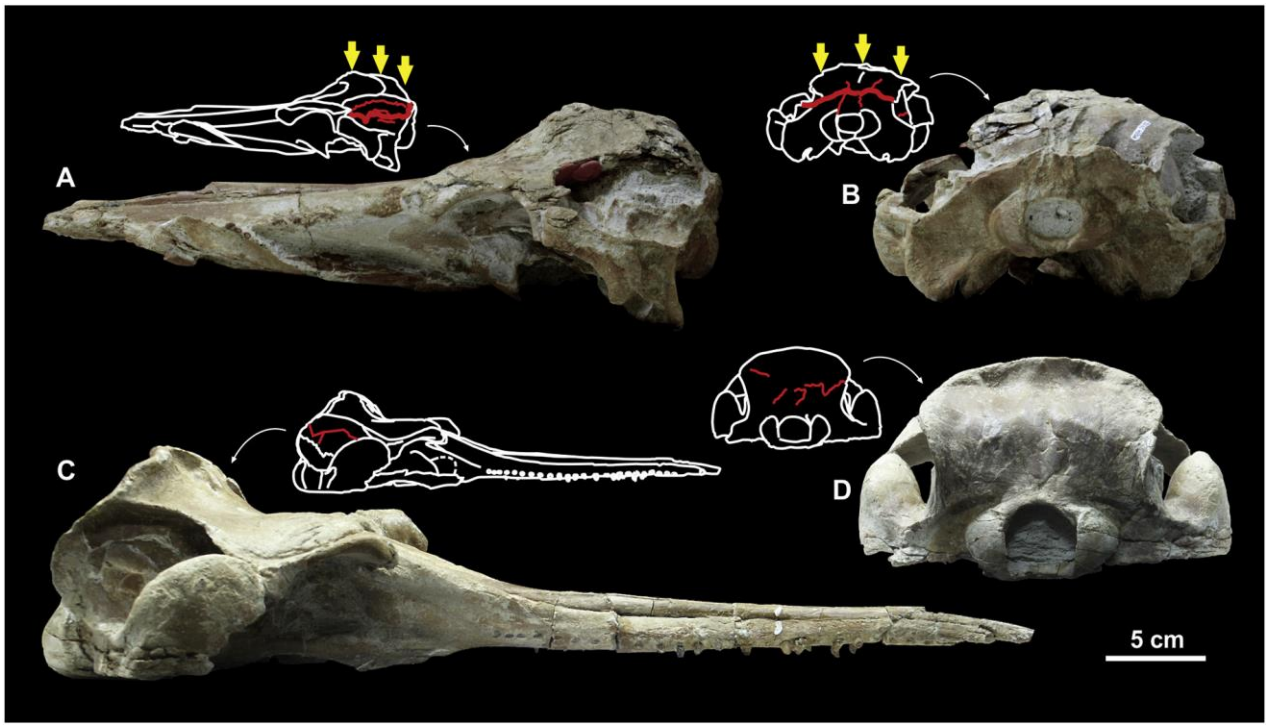

Figure 12

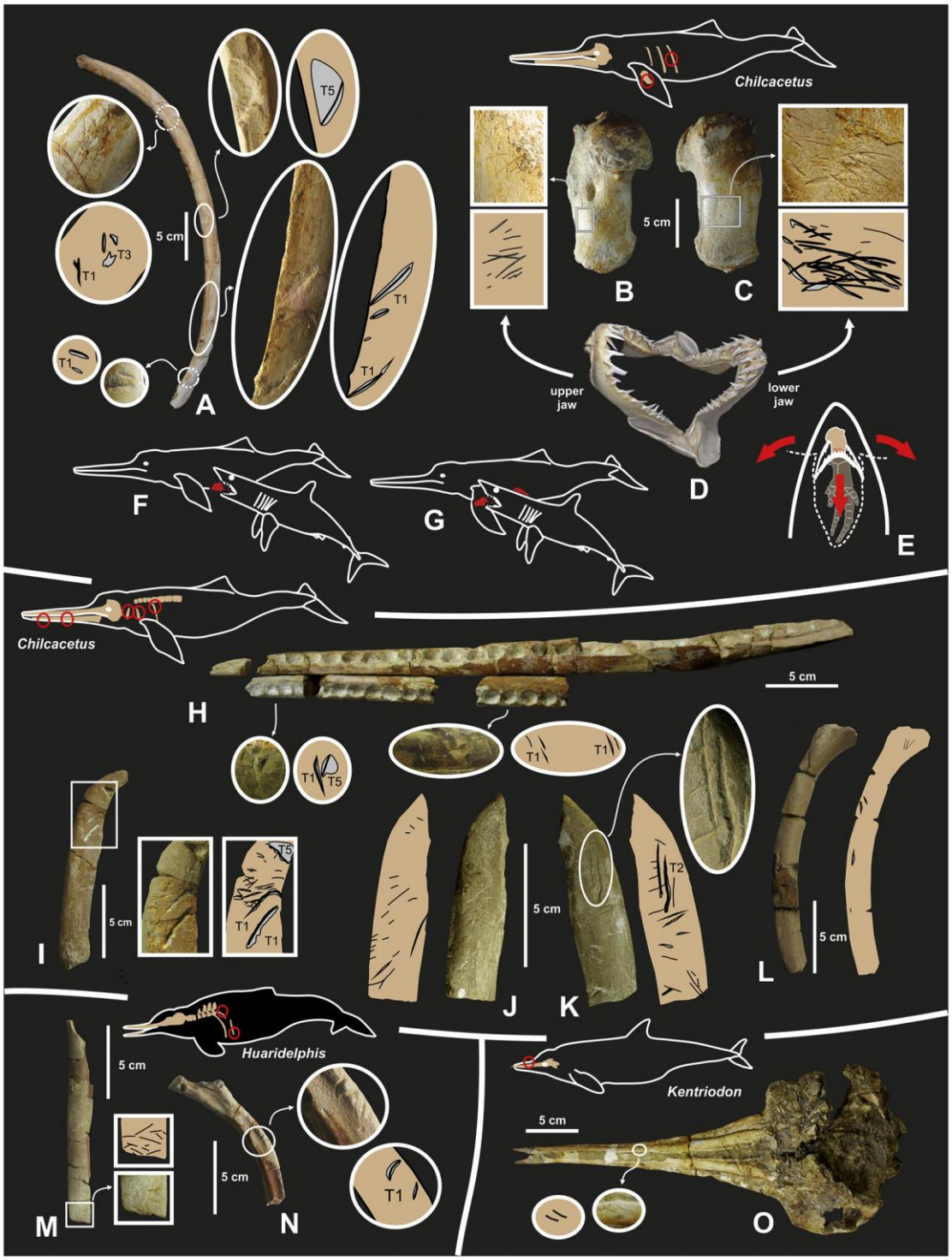

1347

1348 Figure 13

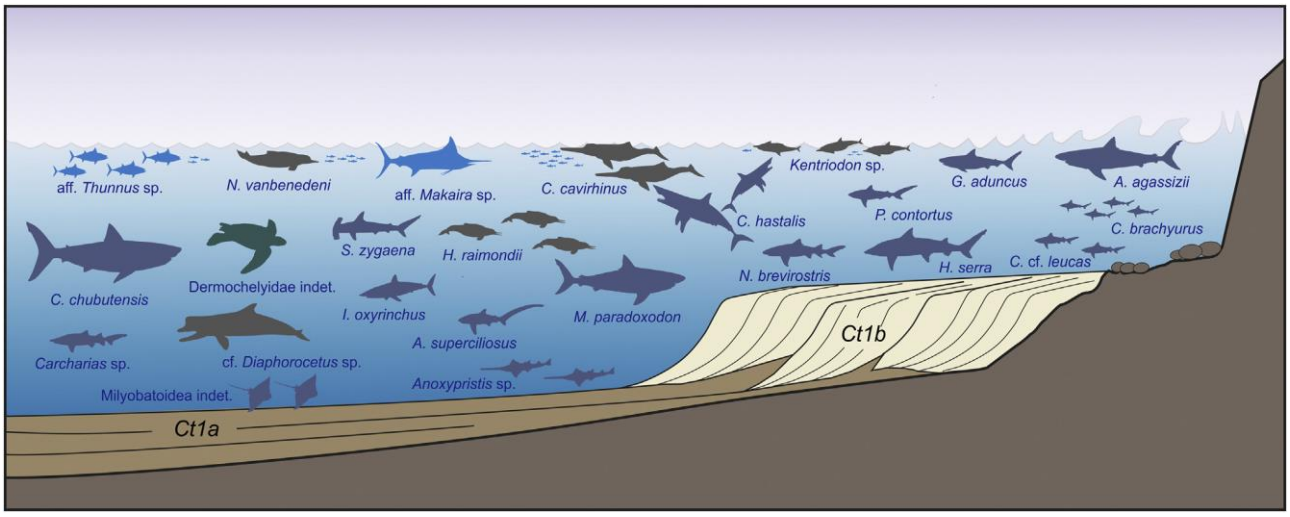

1349

1350 Figure 14

1351

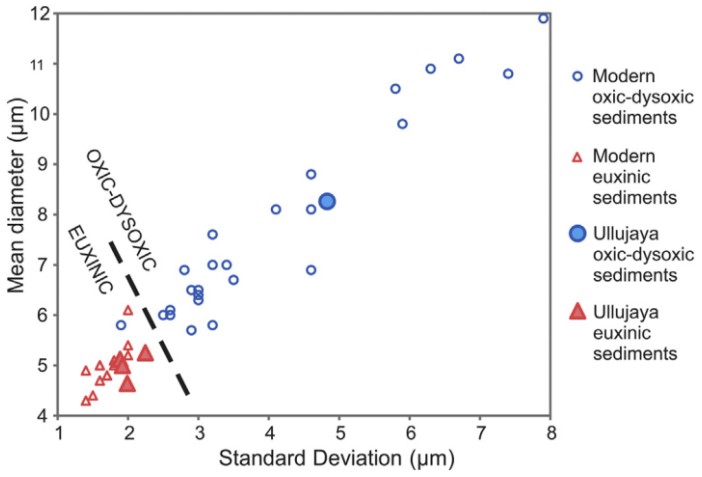

1352

1353 Figure 15

1354

1355

1356

1357

Field number	Height abs (m)	Determination	Preserved bones	In situ	Skull disposition	Skeletal completeness	Bone articulation	Marked recent erosion	Collected and kept at MUSM
Cetacea									
O1	25.9	cf. *Diaphorocetus* sp.	Cranium	Yes	Dorsal	0	0	–	–
O2	23.8	Physeteroidea indet.	Cranium	Yes	Ventral	0	0	–	–
O3	15.0	*Huaridelphis raimondii*	Partial skeleton including cranium, fragmentary mandibles, and some vertebrae and ribs	Yes	–	1	0	–	Yes
O4	27.9	Squalodelphinidae indet.	Partial skeleton including mandibles, humeri, tympanic bulla, and some vertebrae and ribs	Yes	–	2	0	–	In part
O5	9.7	*Chilcacetus cavirhinus*	Partial skeleton including cranium, mandibles, humerus, some vertebrae and ribs	Yes	Dorsal	2	0	–	Yes
O6	15.0	*Chilcacetus cavirhinus*	Partial skeleton including cranium, mandibles and some vertebrae and ribs	Yes	–	1	1	–	Yes
O7	30.8	*Kentriodon* sp.	Cranium	Yes	Ventral	0	0	–	–
O8	15.0	*Kentriodon* sp.	Cranium with tympanic bulla	Yes	–	0	0	–	–
O9	25.5	*Kentriodon* sp.	Cranium	Yes	–	0	0	–	Yes
O10	25.5	*Kentriodon* sp.	Cranium	Yes	–	0	0	–	Yes
O11	28.1	*Kentriodon* sp.	Cranium	Yes	Dorsal	0	0	–	–
O12	17.4	*Kentriodon* sp.	Cranium	Yes	Dorsal	0	0	–	–
O13	14.8	*Kentriodon* sp.	Partial skeleton including cranium and some vertebrae and ribs	Yes	–	1	1	–	–
O14	17.4	*Kentriodon* sp.	Fragmentary cranium	Yes	Ventral	0	0	–	–
O15	23.3	*Kentriodon* sp.	Cranium with ear bones	Yes	Ventral	0	0	–	–
O16	15.0	*Kentriodon* sp.	Cranium, mandibles and portion of postcranial skeleton	Yes	Dorsal	1	0	–	Yes
O17	15.0	*Kentriodon* sp.	Cranium	Yes	–	0	0	–	–
O18	24.1	*Kentriodon* sp.	Fragmentary cranium	Yes	–	0	0	–	–
O19	26.2	*Kentriodon* sp.	Fragmentary cranium	Yes	–	0	0	–	–
O20	27.7	Odontoceti indet.	Fragments of humerus	Yes	–	0	0	–	–
O21	29.2	Odontoceti indet.	Fragmentary cranium	Yes	Ventral	0	0	Present	–
O22	30.8	Odontoceti indet.	Cranium	Yes	Dorsal	0	0	–	–
O23	30.3	Odontoceti indet.	Fragmentary skeleton	Yes	–	1	1	–	–
O24	29.2	Odontoceti indet.	Rostrum, cervical vertebrae, and four thoracic vertebrae	Yes	Dorsal	1	3	–	–
O25	30.8	Odontoceti indet.	Fragmentary cranium	Yes	–	0	0	–	–
O26	25.9	Odontoceti indet.	Fragmentary cranium	Yes	–	0	0	–	–
O27	15.0	Odontoceti indet.	Skull	Yes	Ventral	0	0	–	–
O28	29.2	Odontoceti indet.	Fragmentary rostrum	Yes	Dorsal	0	0	Present	–
O29	15.0	Odontoceti indet.	Mandible, vertebrae and ribs	Yes	–	1	0	–	–
O30	17.4	Odontoceti indet.	Fragmentary cranium	Yes	–	0	0	Present	–
O31	19.6	Odontoceti indet.	Mandible fragment, thoracic vertebrae, ribs, scapula	Yes	–	1	1	Present	–
O32	13.9	Odontoceti indet.	Rostrum fragment	Yes	Ventral	0	0	Present	–
O33	21.7	Odontoceti indet.	Fragments of cranium	Yes	–	0	0	–	–
O34	16.4	Odontoceti indet.	Cranium and ribs	Yes	–	1	0	–	–
O35	21.7	Odontoceti indet.	Cranium	Yes	Dorsal	0	0	Present	–
O36	25.8	Odontoceti indet.	Incomplete atlas and axis	No	–	–	–	–	–
O37	25.5	aff. Odontoceti indet.	Caudal vertebrae	No	–	–	–	–	–
O38	28.1	aff. Odontoceti indet.	Seven vertebrae	Yes	–	1	4	–	–
O39	27.7	aff. Odontoceti indet.	Fragments of vertebrae	No	–	–	–	–	–
O40	27.9	aff. Odontoceti indet.	Lumbar and caudal vertebrae	Yes	–	1	0	–	–
O41	26.2	aff. Odontoceti indet.	Lumbar and caudal vertebrae	Yes	–	1	0	–	–
O42	25.5	aff. Odontoceti indet.	Lumbar and caudal vertebrae	No	–	–	–	–	–
O43	14.8	aff. Odontoceti indet.	Fragmentary vertebrae	No	–	–	–	–	–
O44	14.2	aff. Odontoceti indet.	Fragmentary vertebrae and ribs	Yes	–	1	0	–	–
O45	14.2	aff. Odontoceti indet.	Vertebrae (including atlas and axis) and ribs	Yes	–	1	0	–	–
O46	14.8	aff. Odontoceti indet.	Caudal vertebrae	No	–	–	–	–	–
O47	14.8	aff. Odontoceti indet.	Vertebrae and ribs	No	–	–	–	–	–
O48	17.4	aff. Odontoceti indet.	Vertebrae and ribs	Yes	–	1	0	–	–
O49	17.4	aff. Odontoceti indet.	Eight vertebrae	Yes	–	1	2	Present	–
O50	14.8	aff. Odontoceti indet.	Thoracic vertebrae	Yes	–	1	2	–	–
O51	24.7	aff. Odontoceti indet.	Vertebrae and ribs	Yes	–	1	2	–	–

(*continued on next page*)

Table 1

Table 1 (*continued*)

Field number	Height abs (m)	Determination	Preserved bones	In situ	Skull disposition	Skeletal completeness	Bone articulation	Marked recent erosion	Collected and kept at MUSM
O52	25.9	aff. Odontoceti indet.	Fragmentary vertebrae	No	–	–	–	Present	–
O53	27.4	aff. Odontoceti indet.	Fragmentary vertebrae	No	–	–	–	Present	–
O54	21.1	aff. Odontoceti indet.	Fragmentary vertebrae	No	–	–	–	Present	–
O55	14.2	aff. Odontoceti indet.	Fragmentary vertebrae	No	–	–	–	Present	–
O56	27.9	aff. Odontoceti indet.	Cervical and thoracic vertebre	Yes	–	1	2	–	–
O57	26.2	aff. Odontoceti indet.	Lumbar to caudal vertebrae	Yes	–	1	0	–	–
O58	33.5	aff. Odontoceti indet.	Fragmentary vertebrae	No	–	–	–	Present	–
O59	14.2	Odontoceti indet.	Thoracic vertebrae and ribs	Yes	–	1	2	–	–
O60	25.9	aff. Odontoceti indet.	Vertebrae and ribs	Yes	–	1	2	–	–
O61	25.9	aff. Odontoceti indet.	Vertebrae and ribs	Yes	–	1	0	–	–
O62	25.9	aff. Odontoceti indet.	Lumbar vertebrae and ribs	Yes	–	1	0	–	–
O63	16.4	aff. Odontoceti indet.	Rib	Yes	–	0	0	–	–
O64	26.2	aff. Odontoceti indet.	Axis, thoracic vertebra and rib fragments	Yes	–	1	0	–	–
O65	26.4	aff. Odontoceti indet.	Fragmentary vertebrae	No	–	–	–	Present	–
Testudines									
R1	14.8	Testudines indet.	Fragments of carapax and partial forelimb	Yes	–	1	0	–	–
Osteichthyes									
T1	28.1	aff. *Thunnus* sp.	Skull bone (dentary)	Yes	–	0	0	–	–
T2	29.2	aff. *Thunnus* sp.	Caudal fin	Yes	–	0	4	–	–
T3	26.4	aff. *Thunnus* sp.	Fragment of skull bone (dentary)	Yes	–	0	0	–	–
T4	14.8	aff. *Thunnus* sp.	Vertebrae	Yes	–	1	14	–	–
T5	14.2	aff. *Thunnus* sp.	Thirteen vertebrae	Yes	–	1	2	–	–
T6	14.2	aff. *Thunnus* sp.	Seven vertebrae and rays	Yes	–	1	2	–	–
T7	25.5	aff. *Thunnus* sp.	Partial skeleton	Yes	–	1	2	–	–
T8	25.2	aff. *Thunnus* sp.	Vertebrae	Yes	–	1	2	–	–
T9	25.5	aff. *Makaira* sp.	Vertebrae, skull bones, and other skeletal elements	Yes	–	2	2	–	–
T10	18.2	Osteichthyes indet.	Cranium	Yes	Dorsal	0	0	–	–

Table 1 (continued)

Order	Family or superfamily	Genus and species	Number of specimens
Lamniformes	Odontaspididae	*Carcharias* sp.	2
	Alopiidae	*Alopias superciliosus*	5
		Anotodus agassizii	16
	Otodontidae	*Megalolamna paradoxodon*	1
		Carcharocles chubutensis	30
	Lamnidae	*Isurus oxyrinchus*	88
		Cosmopolitodus hastalis	242
Carcharhiniformes	Hemigaleidae	*Hemipristis serra*	10
	Carcharhinidae	*Physogaleus contortus*	48
		Galeocerdo aduncus	20
		Negaprion brevirostris	2
		Carcharhinus brachyurus	539
		Carcharhinus cf. *leucas*	2
	Sphyrnidae	*Sphyrna zygaena*	1
Myliobatiformes	Myliobatoidea	Myliobatoidea indet.	82
Rhinopristiformes	Pristidae	*Anoxypristis* sp.	2
			1090

Table 2

Number	Height abs (m)	Determination	Analysed bone elements	Bone colour	Bone surface	Bone permineralization
O3	15.0	*Huaridelphis raimondii*	Rib	Reddish	Partially dissolved, with borings	Minor, Fe-oxides/hydroxides
O5	9.7	*Chilcacetus cavirhinus*	Ribs	White to brownish	Intact, no borings	High, calcite and dolomite
O16	15.0	*Kentriodon* sp.	Rib	Pinkish	Intact, no borings	–
O29	15.0	Odontoceti indet.	Bone fragment	Reddish	Partially dissolved, with borings	Moderate, Ca-Mg carbonates
O41	26.2	aff. Odontoceti indet.	Vertebra	White	Worn out[a]	Moderate, Ca-Mg carbonates
O52	25.9	aff. Odontoceti indet.	Vertebra	Reddish to black	Worn out[a]	Moderate, Ca-Mg carbonates
O53	27.4	aff. Odontoceti indet.	Vertebra	Brownish	Worn out[a]	Minor, Ca-phosphate and Fe-oxides/hydroxides

[a] The presence/absence of borings cannot be assessed due to the lack of bone surface.

Table 3

	Ullujaya locality, Chilcatay Fm (Peru) Lower Burdigalian	Arenarie di Belluno (Italy) Upper Aquitanian to Lower Burdigalian	Monte León Fm (Argentina) Aquitanian	Gaiman Fm (Argentina) Lower Burdigalian	Pyramid Hill Sand Member, Jewett Sand Fm (California, USA) Aquitanian	Lower part Calvert Fm and Pungo River Fm (Delaware, Maryland, North Carolina, Virginia, USA) Aquitanian-Burdigalian
Odontoceti						
Physeteroidea						
Physeteridae	cf. *Diaphorocetus* sp.		*Diaphorocetus poucheti*	*Idiorophus patagonicus*		*Orycterocetus crocodilinus*
Physeteroidea indet.		*'Scaldicetus' bellunensis*				
Platanistoidea						
Allodelphinidae					*Allodelphis pratti*	
Dalpiazinidae		*Dalpiazina ombonii*				
Platanistidae						*Araeodelphis natator* *Zarhachis flagellator*
Prosqualodontidae				*Prosqualodon australis*		
Squalodelphinidae	*Notocetus vanbenedeni* *Huaridelphis raimondii*	*Squalodelphis fabianii*	*Notocetus vanbenedeni*			*Phocageneus venustus* Squalodelphinidae indet.
Squalodontidae		*Squalodon bariensis* *Squalodon bellunensis* *Squalodon peregrinus*		*Phoberodon arctirostris*		*Squalodon calvertensis* *Squalodon whitmorei*
Incertae sedis				*Aondelphis talen*		
Eurhinodelphinoidea						
Eurhinodelphinidae		*Mycteriacetus bellunensis* *Ziphiodelphis abeli* *Z. sigmoideus*		Eurhinodelphinidae indet.		*Schizodelphis morckhoviensis* *Xiphiacetus bossi*
Eoplatanistidae		*Eoplatanista italica* *E. gresalensis*				
Eurhinodelphinoid-like						
Incertae sedis	*Chilcacetus cavirhinus*			*Argyrocetus patagonicus*	"*Argyrocetus*" *bakersfieldensis* "*Argyrocetus*" *joaquinensis* *Macrodelphinus kelloggi* *Miodelphis californicus*	
Delphinida						
Kentriodontidae	*Kentriodon* sp.		*Kentriodon* sp.	*Kentriodon* sp.		*Kentriodon pernix* *Delphinodon dividum*
Mysticeti						
Balaenidae				*Morenocetus parvus*		
Cetotheriidae s.l.				*Aglaocetus moreni*		*Parietobalaena palmeri*

Table 4